Implications of Alzheimer's disease on brain insulin and Aβ uptake

Author

Chaitanya Chakravarthi Gali

PhD student (DK-MCD)

Medical University of Graz, Austria.

Supervisor

Prof. Karunya Kandimalla

Internal Supervisor

Prof. Ute Panzenboeck

Host lab

Department of Pharmaceutics, University of Minnesota, Minneapolis, USA.

ACKNOWLEDGEMENTS

I sincerely thank members of (Prof. Karunya Kandimalla group - Department of Pharmaceutics) University of Minnesota and Mayoclinic (Val Lowe., MD. group – Department of Radiology) for their constant support during my stay in Minnesota. Prof. Karunya Kandimalla for designing and modelling SPECT analysis. Specially I would like to acknowledge the support of Geoffry Curran, Tyler J. Brunisma and Paul H. Min for breeding, feeding, and performing insulin tolerance and SPECT studies in APP/PS1 mice.

Contents

ABSTRACT

Loss of brain insulin response is regarded as one of the earliest pathological changes in Alzheimer's disease (AD) brain. This triggers brain insulin resistance, which is being referred to as type-3 diabetes or diabetes of brain. The brain insulin signaling plays a key role in memory consolidation and long term potentiation. Insulin receptors are located in various regions of brain and are responsible for metabolic functions of brain. Blood-brain barrier regulates the entry of peripheral insulin into brain. In the current study, we explored the effects of Aβ on central and peripheral insulin responses in APP/PS1 mice, which were previously shown exhibit low insulin tolerance and inability to metabolize blood glucose. High fat- diet (HFD) feeding further elevated the insulin resistance in APP/PS1 mice. Western blot analyses confirmed dysregulation in brain, liver and vascular insulin signaling in APP/PS1 mice. Uptake studies using ^{125}I-insulin revealed a marked reduction in brain insulin uptake in APP/PS1 mice compared to WT mice. On the other hand, plasma-to-brain trafficking of ^{125}I-Aβ42 decreased in APP/PS1 mice. Furthermore, Peripheral insulin clearance kinetics revealed that APP/PS1 mice clear ^{125}I-insulin and ^{125}I-Aβ faster when compared to WT littermates. In conclusion, our results demonstrate that central insulin resistance in AD severely impair ^{125}I-insulin and ^{125}I-Aβ42 uptake kinetics, whereas, peripheral insulin resistance in APP/PS1 mice elevated ^{125}I-insulin clearance thereby contributing to loss of insulin function.

1. INTRODUCTION

Alzheimer's disease (AD) is a complex neuropathological disease with multiple disease targets. Majorly manifested by amyloid beta (Aβ) (1,2) and/or neurofibrillary tangle (NFT) (3) accumulations in various regions of the brain debilitating its ability to function, and thereby leading to neurodegeneration and memory impairment (4,5,6). Amyloid-β is generated from ~105 kDa transmembrane peptide called amyloid β precursor protein (APP) (7) upon sequential enzymatic cleavage by β-secretase (BACE-1) (8) and γ-secretase (9). APP gene in humans is located on chromosome 21 and generates 8 isoforms upon alternative splicing. The most common isoforms are 695, 751, and 770 amino acid forms (10). More importantly, APP695 is predominantly expressed in nervous tissue and plays important role during neuronal differentiation, whereas the other two isoforms are ubiquitously present in other cell types including microglia and astrocytes (11). APP plays a predominant role in synapse formation, neuronal migration and outgrowth, synaptic plasticity and transmission, memory and learning. Mutations in APP, enzymes involved in APP processing, as well as processed Aβ peptides that aggregate in brain parenchyma and cerebral vasculature could lead to AD or cerebral amyloid angiopathy (CAA) (12,13,14), termed to be the most common variants of Aβ mediated diseases. APP processing generate wide range of Aβ peptides, however, Aβ 1-40 and Aβ 1-42 are the predominant isoforms. Increased in Aβ 1-42/ Aβ 1-40 ratio is known to exacerbate AD (15).

Tau is a major microtubule associated protein (MAP) predominantly expressed in neuronal tissue. So far 2 isoforms of tau were identified (MAP1 & MAP2), located on chromosome 17 and generated by alternate splicing of their pre-mRNA'S (16). Tau promotes assembly of the microtubules by interacting with tubulin, thereby stabilizing the cell structure and intracellular trafficking. Under healthy conditions each tau contains 2-3 moles of phosphate per mole per protein. However under pathological conditions tau is approximately three to four-fold more hyperphosphorylated leading to formation of paired helical filaments known as neurofibrillary tangles (NFT) (17). These hyperphosphorylated NFT filament aggregates to form insoluble complexes in the neuronal cells leading to tauopathies (16,17). Predominantly these processes are modulated by tyrosine kinases such as GSK-3β (Glycogen synthase kinase 3 beta) and cdk5 (cyclin dependent kinase 5) (18). AD human brain autopsies revealed an enhanced correlation with GSK-3β activation and tauopathies (19).

1.1. Implications of Type 2 diabetes on brain insulin signaling:

Type 2 diabetes (T2D) is the major contributor for peripheral insulin resistance (34,36). High-fat diet (HFD) is associated with peripheral insulin and central insulin resistance by modulating the insulin receptor activity, thereby insulin signaling (36). HFD progressively reduces the responsiveness of peripheral tissues to insulin. Furthermore, according to Mayo Clinic AD Patient Registry 80% of AD patients have either T2DM or impaired fasting blood glucose (60). HFD induces central synaptic plasticity and hepatic insulin resistance in mice. Moreover, HFD feeding aggravate the Aβ pathology in AD mice. HFD feeding further effects insulin responses in brain by dampening surface insulin receptor availability, thereby, affecting the ability of insulin receptors to activate kinases such as Akt, S6 and GSK3β involved in cell growth and homeostasis. Whereas, activation of AMPK, which regulates mTOR/Akt signaling thereby downregulating upstream PI3K activity in cells (60).

1.2. Implications of insulin receptors and insulin signaling in the brain:

Insulin receptors (IR) are highly expressed in various regions of the brain, it was shown that insulin regulates cellular metabolism in brain. Insulin actively supply glucose via modulating the GLUT 1 and 3 transporters in the neuronal cells (61). Insulin signaling and its regulation in the brain are broadly elaborated. Insulin signaling is critical for the brain to conserve memory and long term potentiation of neurons. Insulin promote neuronal excitability by regulating the ion channels like calcium and sodium which are critical to relay information across the neuronal cells. Insulin exerts its effects upon binding to the IR and thereby activating receptor bound tyrosine kinase, consisting of two subunits forming heterotetramer upon insulin binding, resulting in activation of insulin receptor substrate (IRS) proteins on tyrosine residues. src-homology-2 (SH-2) domain-containing proteins such as the p85-regulatory subunit of phosphatidyl inositol 3-kinase (PI3K), the growth factor receptor binding protein 2 (Grb 2) and the protein tyrosine phosphatase (Syp) act as the phosphorylation sites are located in domains IRS domains. Protein binding to tyrosine-phosphorylated IRS proteins results in their activation, and initiate downstream activation of the proto-oncogene serine/threonine protein kinase (Ras-Raf-MAPK) cascade or activation of PIP3 serine/threonine kinases. These signals known to effect various biological activities of the cell including inhibition of apoptosis, tau phosphorylation, the regulation of amyloid precursor protein (APP) secretion and the regulation of gene transcription (e.g. of hypothalamic neuropeptides). Insulin uptake studies

using radiolabeled ^{125}I-insulin identified that insulin binding to the IR in certain regions of the brain like basal ganglia, hippocampus, cerebellum, choroid plexus, neocortex, limbic and olfactory regions of the brain (61,62). Since insulin plays a key role in neuronal cell proliferation and differentiation, insulin and insulin receptor mediated signaling is considered a prime importance in neurodegenerative diseases involving memory function.

1.3. Effect of insulin resistance on AD pathophysiology:

Based on resting-state functional magnetic resonance imaging (MRI), AD related dementias have been classified into two major categories namely normal cognitive function, amnestic mild cognitive impairment (aMCI) and AD (20). Currently, no pharmacological therapy is available in the market to treat AD and related complications. Four FDA approved drugs are available to treat AD related symptoms but none of these drugs could prevent the progression of the disease (21). Of several clinical trials that are underway to find potential therapeutics to treat AD (22), insulin Aspart, an insulin mediated intranasal formulation, made it to phase 3 clinical trials, and demonstrated improvement in cognitive functions in AD individuals (22). Recent evidences show that diabetes increases AD risk, and is believed to trigger brain insulin resistance, which is referred to as type 3 diabetes (T3D) (23). Insulin signaling impairment has been related to loss in cognitive ability (24) and insulin is known to evoke excitability in neurons and has been instrumental in long term memory recall (25,26). Disrupted insulin signaling in the brains of AD subjects and various animal models have been reported (27,28). More importantly insulin signaling deficiencies were reported to be early pathological indicative in MCI individuals (29).

Insulin effects Aβ metabolism at different levels which involves altering the enzymes and proteins involved in Aβ production for example in cells expressing APP mutants (APPsw). It was shown that insulin modulate Aβ levels by decreasing beta-secretase (BACE1), and thus decrease secreted C99 fragments produced upon BACE1 cleavage of APP (31). Further, enhanced levels of alpha-secretase or ADAM10 (enzymatic cleavage of APP involved in non-amyloidogenic pathway) and secreted Amyloid precursor protein-α or sAPPα (cleavage product of non-amyloidogenic pathway) was reported in SH-SY5Y neuroblastoma cells (30). It has been reported that insulin treatment improved memory and reduced brain amyloid beta burden in 3XTg-AD mouse model (32). The protective effects of insulin are majorly attributed to decreased production and increased clearance of Aβ (30,32). These actions of insulin on

various pathways that are implicated in AD certainly rise interest towards generating effective therapeutics towards AD (33).

AD closely resembles diabetic phenotype of the brain and various studies have reported cognitive impairment in multiple high fat fed (HFD) mice model (34,36). HFD feeding closely resembles the T2D and metabolic syndrome phenotype in mice models (34,35,36), by demonstrating insulin resistance, hyperinsulinemia, and hyperlipidemia. Further, HFD feeding aggravated the AD pathology by promoting the Aβ accumulations, which further lead to cognitive disabilities in AD mouse models (32,35,36); insulin treatment in these models imparted beneficial effects by reducing the HFD induced Aβ burden to the control levels (32). For instance, various studies in MCI subjects reported improved memory retention and attention with 20 and 40 IU insulin treatment regiments (37,38,39). Several published studies have indicated that hyperinsulinemia increased the risk of AD, and modulated Aβ metabolism in AD brain (40). While multiple studies suggested the beneficial effects of insulin in ameliorating AD pathology, contradictory findings were also reported showing that the deficiency of insulin receptor (IR) (41) and insulin like growth factor receptor (IGF-1R) in the neuronal cells are linked to reduction in Aβ deposits (42,43). Further, it has been reported that the suppression of insulin mediated phosphoinositide 3-kinase (PI3K) activation upon insulin receptor substrate-1 (IRS-1) silencing reduced APP cleavage by reducing both the alpha-secretase and beta- secretase activity in the neuronal cells (41). The mechanisms which regulate the insulin signaling and insulin mediated effects in AD are yet to be understood.

1.4. Blood brain barrier endothelium and cerebrovascular pathology:

Blood brain barrier (BBB) is the critical interface between brain and peripheral circulation. The BBB regulates exit and entry of various xenobiotics and metabolites, and is known to regulate the transcytosis of the AD proteins like Aβ 1-40 and Aβ 1-42 in and out of the brain. This is accomplished with the help of various receptors such as low density lipoprotein receptor-related protein 1 (LRP1) and receptor for advanced glycation end products (RAGE), which regulate exit and entry of Aβ at the BBB, respectively (44,45,46). LRP-1 knock out at the BBB demonstrated severe accumulations of Aβ in the brain and in the vasculature and aggravated AD in mice. It has been shown that age related dementias compromise BBB function, thereby inability to mediate Aβ clearance. Moreover, cerebral amyloid angiopathy (CAA) may lead to leaky vasculature thereby leading to blood loss and clotting in the brain, inducing cerebral stroke in CAA patients. Insulin is known to regulate the surface mobilization of the LRP-1 at

the BBB (48) and at the periphery (49) thereby contributing to the Aβ clearance. Thus, insulin regulates Aβ clearance from the brain by differentially trafficking Aβ 1-40 and 1-42 at the BBB and modulate the Aβ clearance from the brain in healthy mice (48), and by regulating insulin degrading enzyme (IDE) in the neuronal cells (47).

1.5. Blood brain barrier in brain insulin uptake:

Insulin is the key hormone regulating peripheral and central energy metabolism. Insulin plays a key role in cellular homeostasis and growth via regulating cell survival and growth pathways, which are regulated primarily by PI3K and MAPK pathways. Recent findings suggest that insulin receptors are located in various regions of the brain, plays a vital role in preserving memory and long-term potentiation (LTP). Highly dense regions of Insulin receptors are primarily located on the luminal side of the BBB. Recent findings suggest that insulin is take up via the BBB through receptor mediated endocytosis, prominently require lipid-raft mediated endocytosis. Since insulin mediates predominant effects on learning and memory in the brain, understanding the regulation of peripheral insulin uptake by the brain under AD conditions might help us understand the cause of insulin resistance in AD.

The main purpose of our studies conducted in WT and APP/PS1 mice is to understand the implications of insulin exposure and insulin resistance on peripheral, microvascular and central insulin resistance, and how it impacts AD pathology. Contribution of the BBB in Aβ trafficking under AD conditions. To address this complex phenomena, we applied molecular biology investigations in conjunction with pharmacokinetic modeling using Single-photon emission computed tomography (SPECT) imaging to assess the Aβ clearance from the transgenic wildtype and APP/PS1 Swe age matched littermates.

2. METHODS:

2.1. Animals and housing:

APP/PS1 mice and their non-transgenic littermates were purchased from the Jackson Laboratories (Bar Harbor, ME) and were shipped to animal holding facilities at 2 months of age. Animals were caged in social housing with normal diurnal light variation in a climate-controlled environment. All mice were maintained on a normal laboratory diet until six months of age at which point standard diet was switched to a high fat (60% saturated fat) diet. Feeding of the respective diets continued for 16 weeks. All mice were weighed bimonthly to assess weight gain and/or maintenance. On the day of terminal experimentation, animals were fasted for four hours and sacrificed with an overdose of isoflurane.

2.2. Insulin tolerance tests:

Four and sixteen weeks after starting high fat feeding or continuing regular chow feeding, all mice underwent insulin tolerance testing according to prior reports (52,54). Prior to testing mice were fasted for four hours and tails were cut to allow for blood collection. Fasting blood samples were collected and an intra-peritoneal injection of DOSE insulin (Humilin, COMPANY CITY STATE) was administered. Serial blood samples were collected 15, 30, 60, and 120 minutes after injection. All blood samples were analyzed in real time using a glucometer with single use test strips.

2.3. Harvesting the vital organs and brain:

Animals were fasted for 4h, a bolus IP dose of 2 IU/ kg insulin was administered. Twenty minutes after injection animals were sacrificed under deep anesthesia, and brain vasculature was cleared via intra-cardiac cold PBS perfusion. Vital organs were harvested along with the brains and were immediately frozen on dry ice until processed. Brains were immediately transferred in to HBSS (Hanks balanced salt solution) supplemented with HEPES, protease and phosphatase inhibitors on ice to preserve the phosphorylation events.

2.4. Isolation of the brain microvasculature:

Brain microvasculature was harvested according to the (51) with few modifications. In brief, harvested brains were cleared of meninges by rolling it briefly on a sterile tissue paper and were cleared of cerebellum and medulla oblongata using a scalpel. The cerebral cortices from each mouse were minced using a scalpel blade and all the contents were transferred in to a douncer with a piston and the minced tissue was homogenized with 10 gentle strokes using

MCDB131 medium supplemented with HEPES, protease and phosphatase inhibitors. The homogenate was centrifuged at 2500 G for 10 min in swinging bucket centrifuge at 4^0C. The myelin rich supernatant was discarded and the vessel pellets were dissolved in 2 mL of MCDB131 medium and the suspension was thoroughly mixed with dextran solution (150,000) which is density adjusted to 1.06 g/L with HBSS. The suspension was then centrifuged at 4500 G for 15 min with brake off in a swinging bucket centrifuge to isolate the neuronal tissue from the vasculature. The myelin supernatant was discarded and the pellet was resuspended in 200 µL of HBSS supplemented with 1X protease and phosphatase cocktail. The homogenate is passed through the 180 µM nylon filter and washed with excess HBSS. The vessels retained on 180 uM filter are considered as macrovessel fraction and were fixed with PFA (Paraformaldehyde) 4% and stored at 4^0C, while the filtrate was centrifuged at 10,000 RPM to collect the microvessel fraction. The pellet was immediately lysed with the protein lysis buffer (RIPA buffer) supplemented with protease and phosphatase inhibitors and stored at -80^0C until further use.

2.5. Western Immunoblotting:

Protein quantification was performed using bicinchoninic acid assay (BCA, ThermoFisher Scientific). Samples were mixed with XT loading buffer (Bio-Rad) and proteins were denatured at 90°C for 5 min. Proteins were separated under reduced conditions on SDS-PAGE gel electrophoresis using 1X MOPS or MES buffer (NuPage® Novex 4-12% Bis-Tris Midi Gels). Then, proteins were electroblotted on to 0.2 µm Nitrocellulose membrane (GE Healthcare). Membranes were blocked with 5% not-fat dry milk protein (Bio-Rad) for 1 h at RT. Followed by primary antibody incubations at 4^0c overnight and secondary antibody incubations for 1h at RT (room temperature) with 3X TBS-T (Tris buffer saline with 0.5% tween) wash between each step, blots were detected using Clarity Western ECL Substrate (ThermoFisher Scientific) and a Chemiluminescence Imaging System (Azure Biosystems).

2.6. Preparation of ^{125}I-labeled soluble Aβ42:

The Aβ42 was synthesized as described in our earlier reports (Kandimalla et al., 2005) (52) and the monomers were prepared according to the procedure described by Lacor (Lacor et al., 2004) (53). The Aβ monomers were separated by size exclusion chromatography (SEC) on a Superdex 75 HR10/30 column (GE Healthcare, Piscataway, NJ, USA) and labeled with ^{125}I using the chloramine-T reaction. The unconjugated 125I was removed by overnight dialysis, and the

purity of ^{125}I-labeled protein was determined by trichloroacetic acid (TCA) assay as described previously (Poduslo et al., 2001) (54).

2.7. Preparation of ^{125}I-labeled insulin:

Insulin was labeled with ^{125}I using the chloramine-T reaction (Kandimalla et al., 2005). The unconjugated ^{125}I will be removed by overnight dialysis, and the purity of ^{125}I -labeled protein will be determined by trichloroacetic acid (TCA) assay as described previously (Poduslo et al., 2001) (54).

2.8. Plasma-to-brain ^{125}I-insulin uptake in WT and APP/PS1 mice:

To assess plasma to brain delivery of insulin in WT and APP/PS1 mice, the femoral vein as well as artery was catheterized under general anesthesia. Intravenous bolus administration of 100 µCi of ^{125}I-insulin was administered to each mouse via femoral vein. Immediately after the injection, the mouse was imaged by dynamic single photon emission computed tomography/computed tomography (SPECT/CT) to obtain twenty 15-s frames, twenty 30-s frames, fifteen 1-min frames for a total of 30 min. At the end of experiment, blood was collected in EDTA anticoagulant tubes and the mouse was transcardially perfused with excess PBS followed by 10% neutral buffered formalin. The uptake 125I-inuslin into brain and peripheral organs such as liver and kidney were assessed.

2.9. ^{125}I-insulin plasma pharmacokinetics in WT and APP/PS1 mice:

Mice were anesthetized using 1.5% isoflurane with 4 l/min O_2, and the femoral vein/artery and internal carotid artery were catheterized. Intravenous bolus injection of 100 µCi of ^{125}I-insulin was administered to each mouse via femoral vein. A 20 µl blood sample was collected from the femoral artery at pre-determined time points (0.25, 1, 3, 5, 7, 10, and 15 min); the plasma was separated and TCA precipitated, and the radioactivity of the intact protein was measured in the pellet by a two-channel gamma counter (Cobra II; Amersham Biosciences Inc., Piscataway, NJ). The mouse was transcardially perfused with excess PBS to flush radioactivity in the blood, and the brain radioactivity was assayed and normalized per gram of tissue. The brain tissue was further processed on ice, and gel electrophoresis was run on the residual brain tissue to assess the extent of intact 125I-insulin.

2.10. Plasma-to-brain ^{125}I-Aβ uptake in WT and APP/PS1 mice:

To assess the insulin response on plasma-to-brain Aβ trafficking in WT and APP/PS1 mice, the femoral vein/artery as well as the internal carotid artery of each mouse was catheterized under general anesthesia. Following anesthesia, 500 µCi of ^{125}I-Aβ42 was administered to each mouse via femoral vein. Immediately after the injection, the mouse was imaged by dynamic SPECT/CT to obtain twenty 15-s frames, twenty 30-s frames, fifteen 1-min frames for a total of 30 min. At the end of experiment, blood was collected in EDTA anticoagulant tubes and the mouse was transcardially perfused with excess PBS followed by 10% neutral buffered formalin. The brain and peripheral organs were harvested and the histological analysis will be conducted to assess, amyloid burden and inflammatory changes. The rate of uptake of ^{125}I-Aβ42 into brain and peripheral organs such as heart were assessed.

2.11. ^{125}I-Aβ plasma pharmacokinetics in WT and APP/PS1 mice:

Mice were anesthetized using 1.5% isoflurane with 4 l/min O_2; their femoral vein/artery and internal carotid artery were catheterized. Following anesthesia, 100 µCi of ^{125}I-Aβ42 was administered to each mouse via femoral vein. A 20 µl blood sample was collected from the femoral artery at pre-determined time points (0.25, 1, 3, 5, 7, 10, and 15 min); the plasma is separated; TCA precipitated; and the radioactivity of the intact protein is measured in the pellet by a two-channel gamma counter (Cobra II; Amersham Biosciences Inc., Piscataway, NJ). Then the mouse was transcardially perfused with excess PBS to flush radioactivity in the blood; the brain radioactivity was assayed; and normalized per gram of tissue.

2.12. Kinetic data analysis:

The plasma data was fitted with a biexponential equation and the model parameters were predicted (52).

Ct = A e^{-at} + B e^{-bt} (1), where Ct = ^{125}I-insulin or ^{125}I-Aβ plasma concentration of (µCi/ml); A and B are the intercepts; and α and β are the slopes of the biexponential curve. These parameters were used to simulate the plasma concentration for various SPECT/CT time points, and were employed to determine Patlak influx, Ki. Another quantitative measure of plasma-brain permeability, permeability surface area product (PS) was determined from the plasma pharmacokinetic data by employing the equation provided below:

PS = $\frac{A_{Br}}{\int_0^t C_p}$ (2), where ABr= amount of brain ^{125}I-insulin or ^{125}I-Aβ and $\int_0^t C_p$ = plasma area u.

2.13. Western blot data analysis:

Band intensities were normalized with respective housekeeping controls with the help of image acquisition software ImageJ©. All the statistical analyses were performed using GraphPad Prism software (GraphPad Software, Inc., La Jolla, CA). Two-tailed student's unpaired t-test or one-way ANOVA followed by posthoc "Dunnett's multiple comparisons test" was used to analyze differences between groups. $p<0.05$ was considered statistically significant. All data are presented as means ± SEM. Number of mice used (N) were indicated under respective figure legends.

3. RESULTS:

3.1. Impaired insulin tolerance in APP/PS1 and HFD fed mice:

AD is often termed as type-3 diabetes (diabetes of brain). Considering the impact of AD on brain insulin resistance, we evaluated the effect of APP/PS1 transgene on peripheral insulin resistance. Feeding the Non-transgenic (NTg) and APP/PS1 mice with the HFD diet for 16 weeks significantly increased the body weight (BW) ($P<0.05$) (Figure 1A) and reduced the tolerance towards insulin (Figure 1B & C) in male mice. HFD feeding enhanced BW in female mice of both the genotypes (Figure 1D). Surprisingly, HFD fed female mice were protected from insulin intolerance up on ITT (Figure 1E) unlike APP/PS1 female mice (Figure 1F). Further, significant increase in fasting blood glucose levels upon HFD feeding were observed in both the genotypes and sexes (Figures 2D & 3D). Interestingly, ITT in fasted mice resulted in a significant intolerance towards insulin in APP/PS1 male mice when compared to NTg chow fed mice (Figures 2A & C). HFD feeding further worsened tolerance towards administered insulin in both the genotypes, however, male APP/PS1 mice demonstrated significantly increased insulin intolerance compared to HFD fed NTg mice (Figures 2B & C). No intolerance towards insulin up on ITT was observed in chow fed APP/PS1 mice and HFD fed NTg mice (Figures 3A & C). Interestingly, female APP/PS1 mice demonstrated worsened insulin tolerance up on HFD feeding (Figures 3B & C).

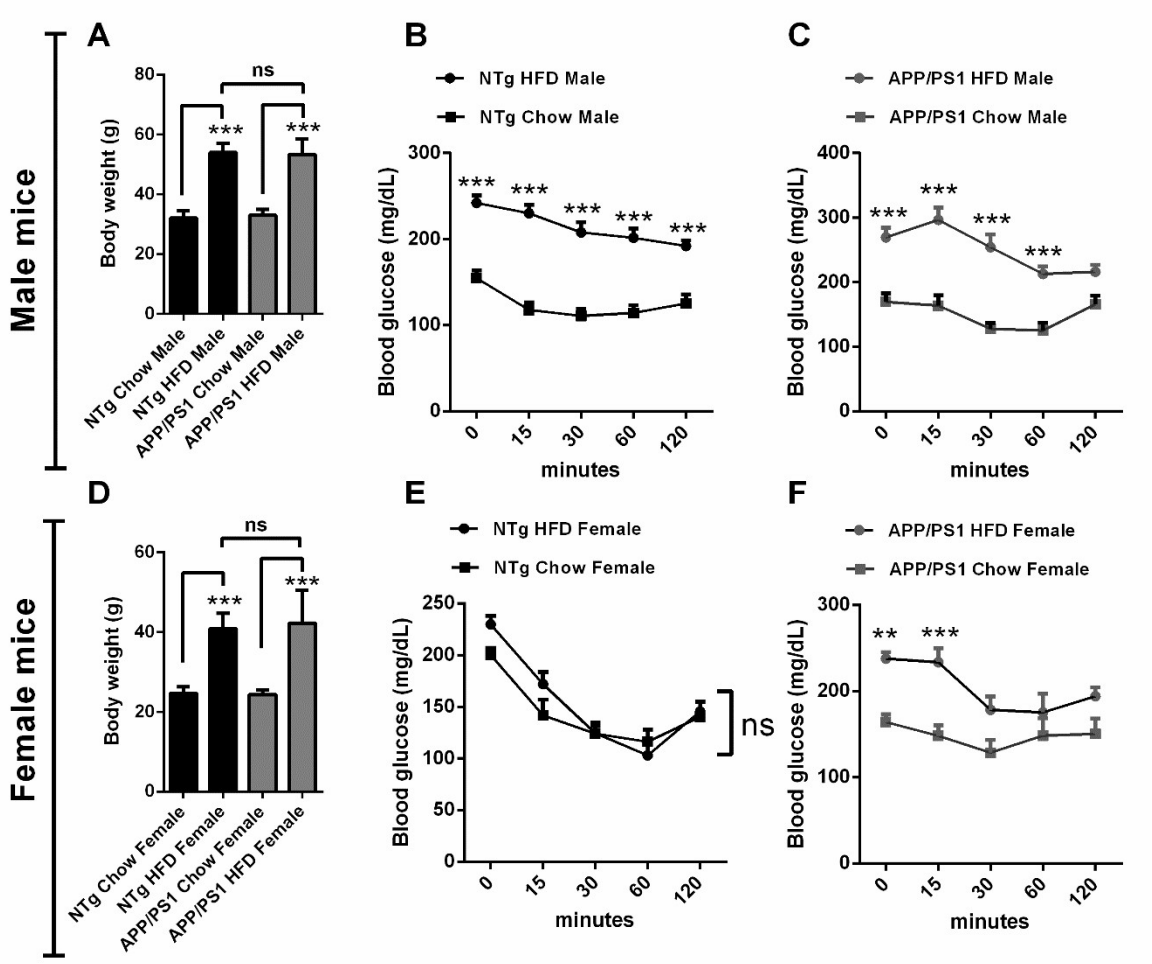

Figure 1: At the end of 16 week feeding, mice were fasted for 4 h and ITT assay was performed. Body weights at the end of 16 week feeding in male and female mice of both the genotypes and feeding regimens (A & D), Plasma glucose levels were monitored in regular diet and HFD fed mice of both the genotype NTg male and female (B & E), APP/PS1 male (C & F). Data represent mean±SEM; N=10 mice/group. Significant differences between the groups were calculated using two-tailed, unpaired students t-test; ***p<0.001. For 1B, 1C, 1E & 1F two-way ANOVA, followed by Dunnet's post-hoc test was applied; **p<0.01 and ***p<0.001.

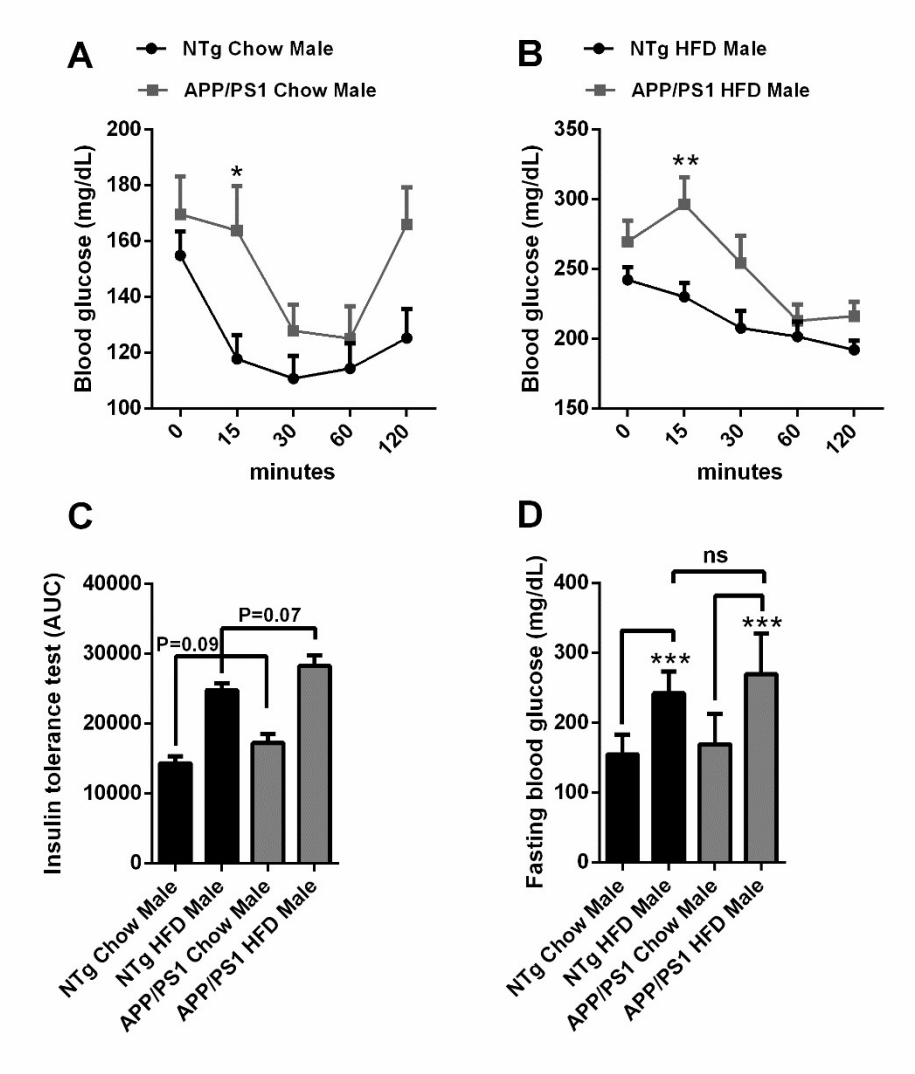

Figure 2: At the end of 16 week feeding, mice were fasted for 4 h and ITT assay was performed. Plasma glucose levels were monitored in male mice of both the genotypes and feeding regimens (A & B). Area under the curve (AUC) for figures A & B (C). Fasting blood glucose in male mice of both the genotypes (D). Data represent mean±SEM; N=10 mice/group. Significant differences between the groups were calculated using two-tailed, unpaired students t-test; ***p<0.001. For 1A & 1B two-way ANOVA, followed by Dunnet's post-hoc test was applied; *p<0.05 and **p<0.01.

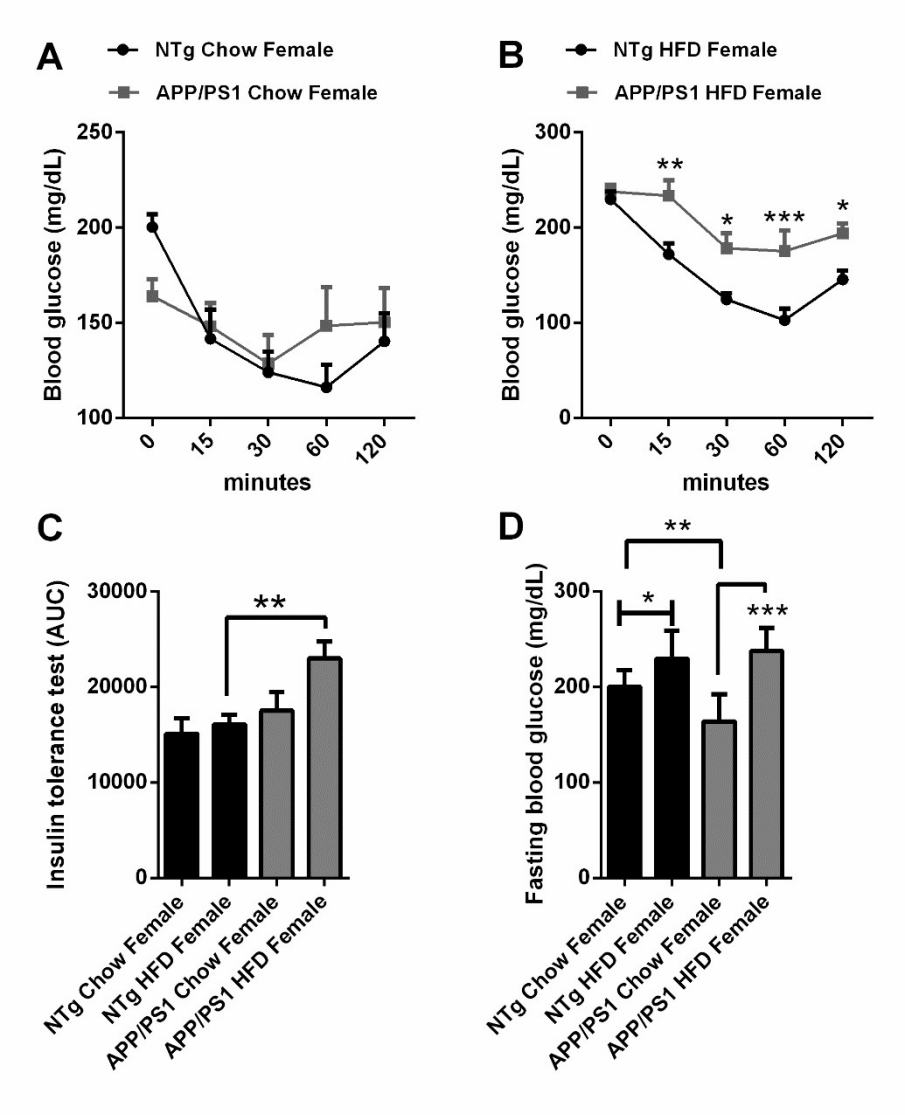

Figure 3: At the end of 16 week feeding, mice were fasted for 4 h and ITT assay was performed. Plasma glucose levels were monitored in female mice of both the genotypes and feeding regimens (A & B). Area under the curve (AUC) for figures A & B (C). Fasting blood glucose in female mice of both the genotypes (D). Data represent mean±SEM; N=10 mice/group. Significant differences between the groups were calculated using two-tailed, unpaired students t-test; *p<0.05, **p<0.01 and ***p<0.001. For 1A & 1B two-way ANOVA, followed by Dunnet's post-hoc test was applied; *p<0.05, **p<0.01 and ***p<0.001.

3.2. Dose ranging studies to identify the optimal dose for insulin administration:

Next we aimed to understand the effects of insulin administration on central and peripheral insulin signaling in APP/PS1 and NTg mice. For finding the relevant dose, dose ranging studies were performed using saline, 1 IU/ Kg insulin (human insulin) & 2 IU/ Kg body weight (BW) insulin for 20 minutes in wildtype (WT) mice. Both the doses activated the downstream insulin signaling in peripheral (Liver and Microvasculature) as well as central compartments (Brain), captured using pAKT (S473) as a read out (Figures 4A – C). Whereas, 2 IU/ Kg BW yielded robust activation of pAKT in both the compartments.

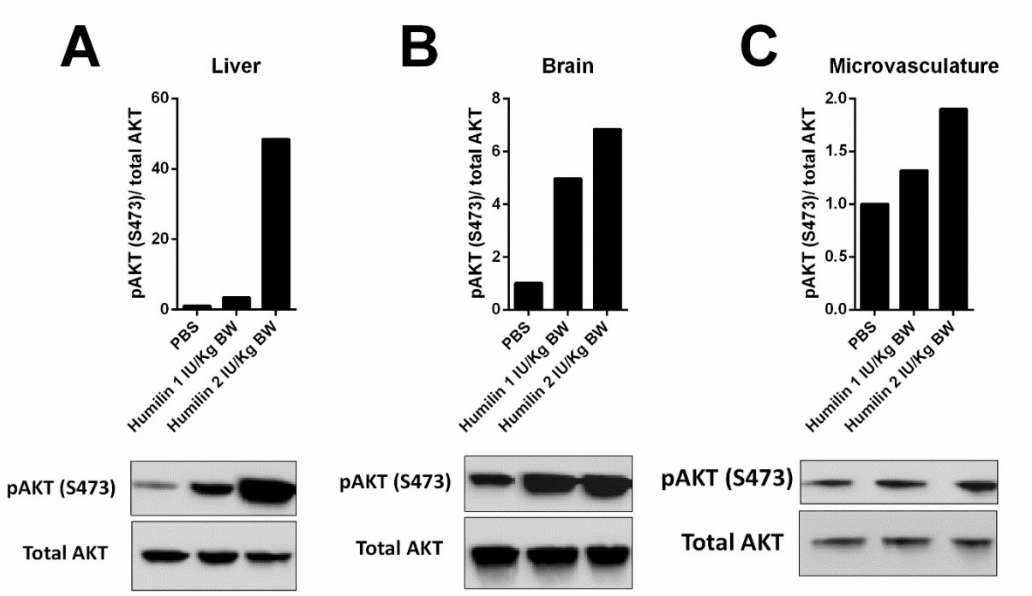

Figure 4: Dose ranging studies with 1 and 2 IU/Kg were performed in NTg age. Twenty minutes after insulin (IP) administration, mice were sacrificed and vital organs were removed, proteins were isolated and subjected to western analysis. Quantitative analysis was performed using ImageJ©. pAKT (S473)/total AKT levels were analyzed using respective antibodies. A) Liver profile, B) Brain profile & C) microvasculature profile.

3.3. HFD feeding perturbed liver insulin responses in APP/PS1 and HFD fed mice:

To understand the impact of AD transgene and HFD feeding on peripheral insulin resistance. After saline or insulin injection for 20 minutes, livers were harvested and were analyzed for insulin signaling events using necessary antibodies. HFD feeding perturbed IR-β levels in saline treated male mice of both the genotypes (Figure 6B), similar but not a significant reduction in IR-β levels were observed in female mice of both the genotypes (Figure 6J). However, upon insulin injection a significant down regulation of both IR-β and IRS-1 levels were observed in HFD fed male mice (Figure 6F & N). Interestingly, insulin stimulation further dampened IRS-1 levels in APP/PS1 chow diet fed male mice (Figure 6E), which demonstrates an insulin resistant peripheral environment in APP/PS1 male mice. HFD fed NTg female mice demonstrated IR-β dysregulation alone with no changes in IRS-1 levels when compared to APP/PS1 female mice (Figures 6M & N). APP/PS1 transgene render female mice to be more susceptible to HFD mediated insulin resistance (Figures 6M & N). HFD feeding resulted in increased pAKT levels in saline treated NTg mice of both the sexes (Figures 6C & K). However, insulin stimulation significantly reduced the pAKT levels compared to chow fed NTg mice (Figures 6G & O). HFD feeding enhanced pAKT levels in female APP/PS1 mice, upon insulin stimulation these increase pAKT levels were reduced to the control levels (Figures 6K & O). Similar changes in pGSK-3 profile was observed in male and female mice of both the genotypes (Figures 6D & L), insulin stimulation further downregulated the activated levels of GSK-3 in both the sexes, which are under the influence of HFD (Figures 6H & P).

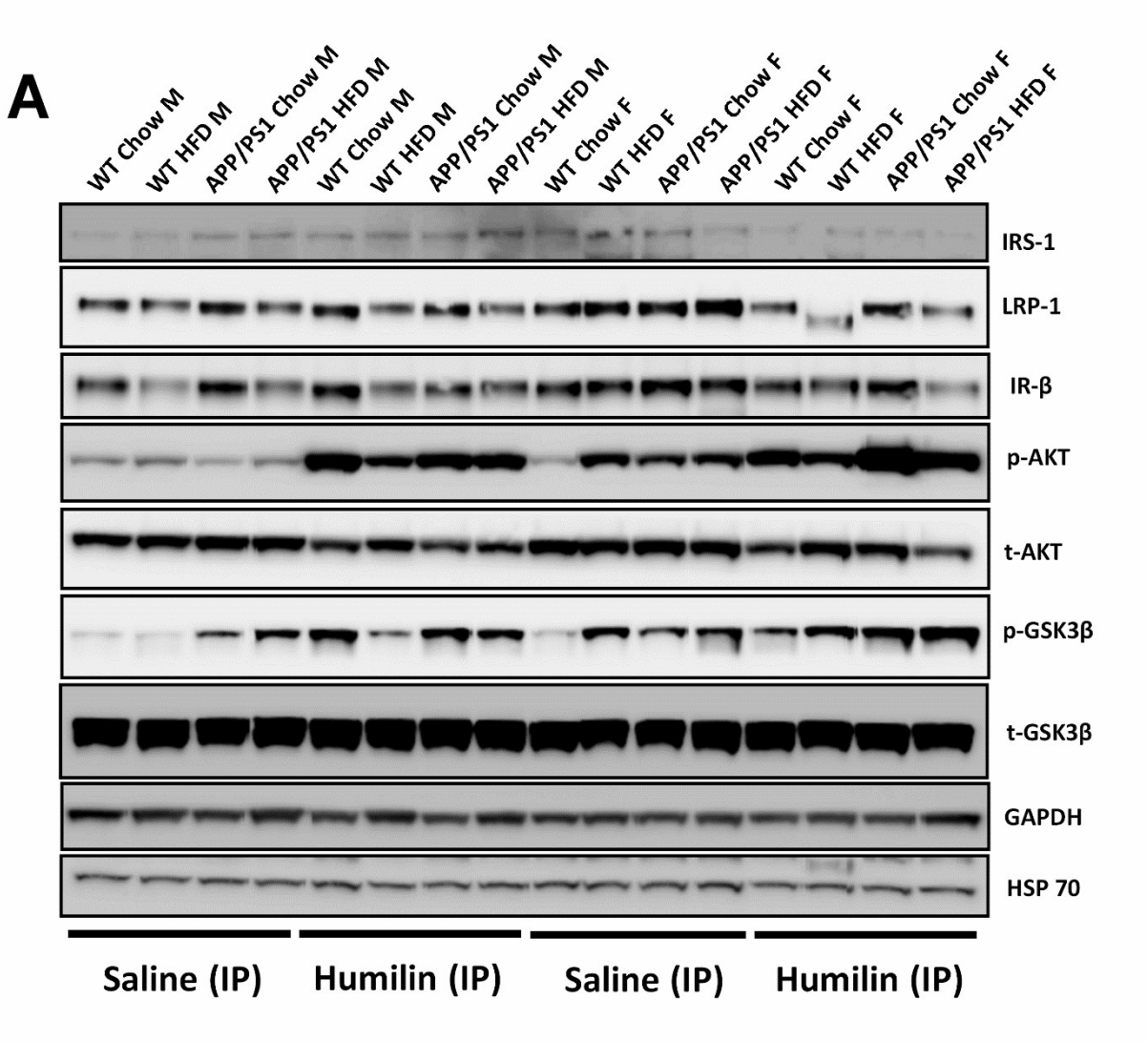

Figure 5: At the end of 16 week feeding, Male and female; APP/PS1 and NTg mice were administered with either 2 IU/Kg insulin or saline (IP) for 20 minutes, animals were sacrificed, vital organs were harvested, proteins were isolated and subjected to western blotting, analyzed for proteins involved in insulin signaling. Representative western blots of liver insulin signaling was demonstrated in figure 5.

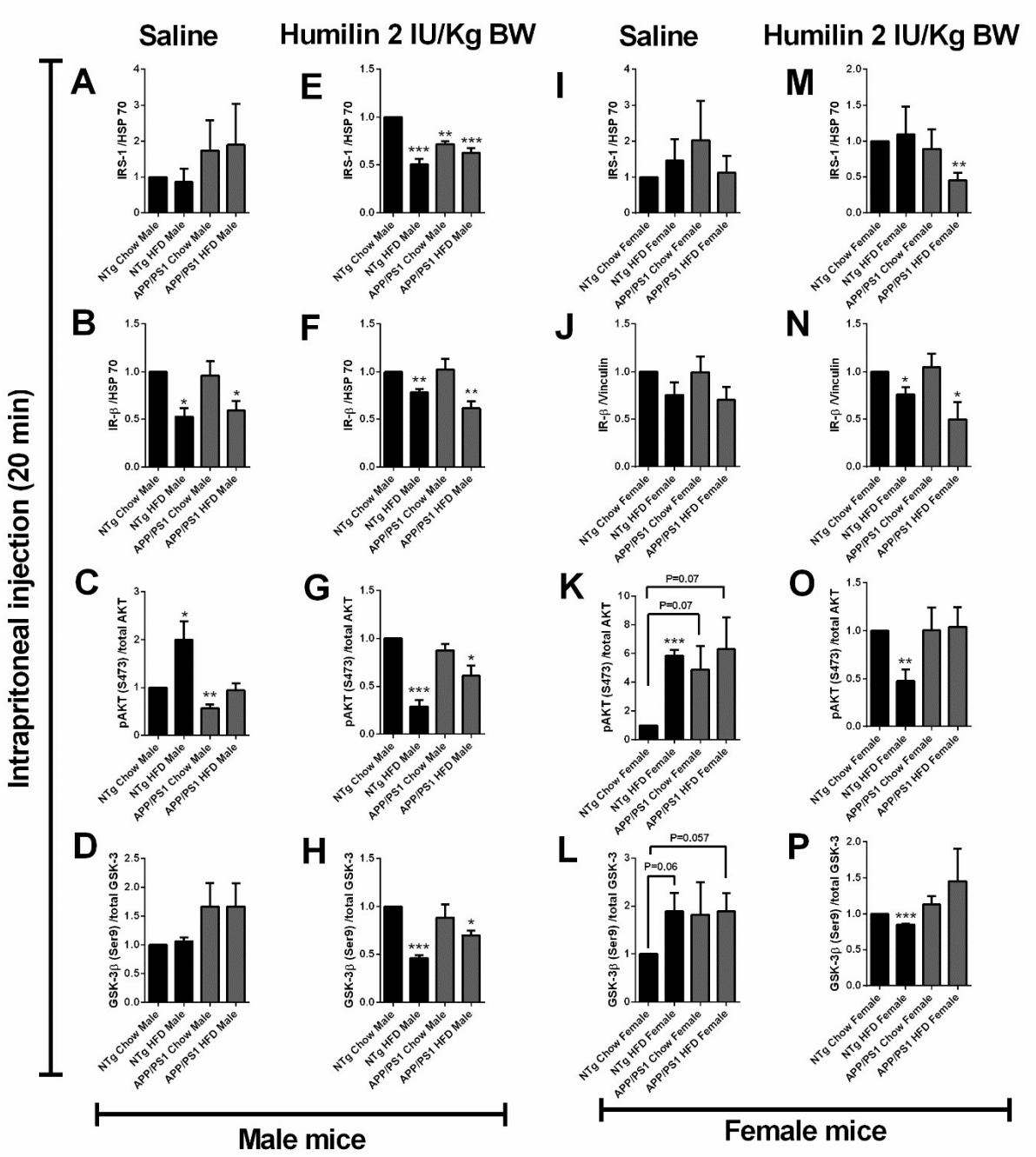

Figure 6: At the end of 16 week feeding, Male and female; APP/PS1 and NTg mice were administered with either 2 IU/Kg insulin or saline (IP) for 20 minutes, animals were sacrificed, vital organs were harvested, proteins were isolated and subjected to western blotting, analyzed for proteins involved in insulin signaling. Quantitative analysis of figure 5 was performed using ImageJ©. IRS-1/HSP-70 (A, E, I & M), IR-β/HSP-70 or Vinculin (B, F, J & N), pAKT (S473)/total AKT (C, G, K & O) and GSK-3β (Ser9)/total GSK-3 (D, H, L & P). Significant differences between the groups were calculated using two-tailed, unpaired students t-test; *p<0.05, **p<0.01 and ***p<0.001.

3.4. APP/PS1 and HFD fed mice displayed impaired brain insulin signaling:

To understand the implications of APP/PS1 transgene and HFD on brain insulin signaling, at the end of 16 weeks feeding study, animals were injected with either saline or insulin (2 IU/ Kg BW) for 20 minutes, brains were harvested and brain lysates were subjected to western blot analysis and were detected for insulin signaling events using relevant antibodies and the densities were normalized with respective loading controls to analyze the differences. Under the basal/ saline administered (unstimulated) conditions, APP/PS1 male mice demonstrated significantly low IRS-1 phosphorylation ($P<0.05$) with no major differences in downstream signaling when compared to NTg mice of chow and HFD feeding regimen (Figure 8A – E). However, insulin administration diminished the phosphorylation of various signaling events including IRS-1, IR-β and ERK in transgenic as well as HFD male mice (Figure 8F – J). Further, we noticed an increase in GSK-3 phosphorylation up on insulin administration in HFD mice of both the genotypes (Figure 8I). No significant changes in brain insulin signaling events were observed in saline administered female APP/PS1 and HFD fed mice when compared to NTg mice (Figure 8K –O). Similar to male mice, downregulation in phosphorylation of IRS-1 and IR-β were observed in APP/PS1 and HFD fed female mice upon insulin administration (Figures 8P & Q). Surprisingly, opposed to male mice a significant down regulation of the GSK-3 phosphorylation was observed in APP/PS1 mice upon insulin administration. Whereas, no significant changes were observed in phosphorylation of major downstream signaling events such as pAKT and pERK (Figures 8R & T).

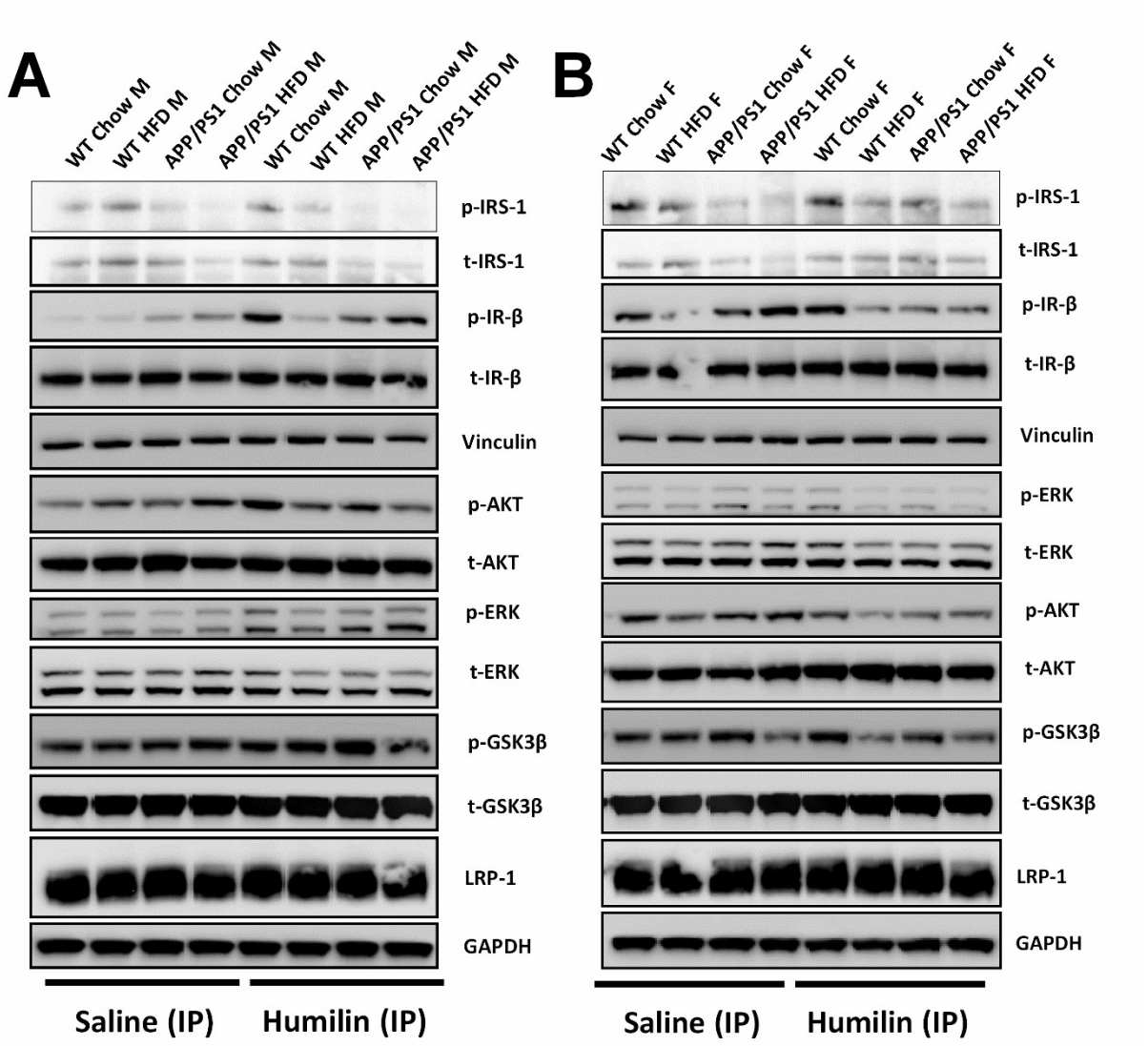

Figure 7: At the end of 16 week feeding, Male and female; APP/PS1 and NTg mice were administered with either 2 IU/Kg insulin or saline (IP) for 20 minutes, animals were sacrificed, vital organs were harvested, proteins were isolated and subjected to western blotting, analyzed for proteins involved in insulin signaling. Representative western blots of brain insulin signaling was demonstrated in figure 7.

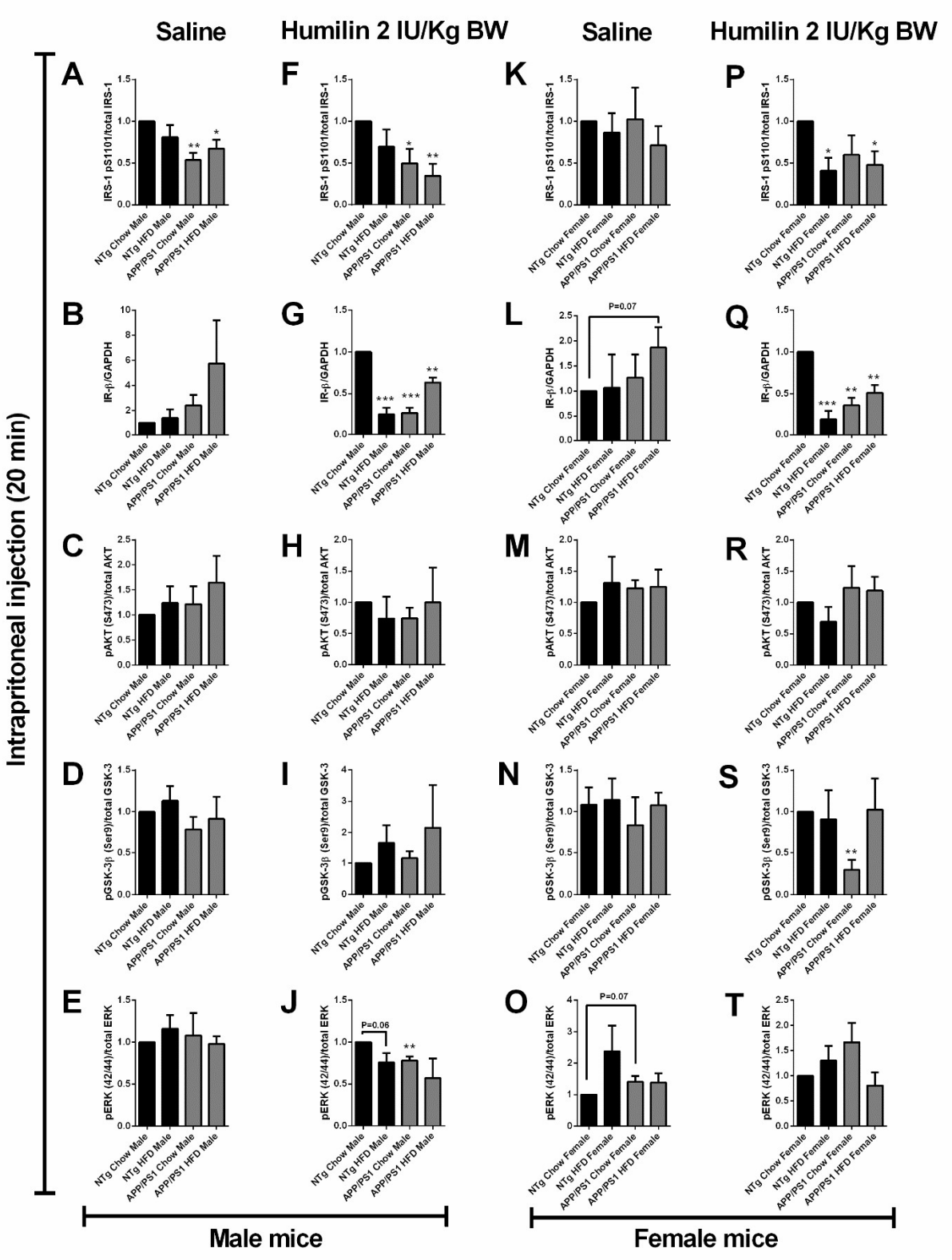

Figure 8: At the end of 16 week feeding, Male and female; APP/PS1 and NTg mice were administered with either 2 IU/Kg insulin or saline (IP) for 20 minutes, animals were sacrificed, vital organs were harvested, proteins were isolated and subjected to western blotting, analyzed for proteins involved in insulin signaling. Quantitative analysis of figure 7 was performed using ImageJ©. pIRS-1 (S1101)/total IRS-1 (A, F, K & P), IR-β/GAPDH (B, G, L & Q),

pAKT (S473)/total AKT (C, H, M & R), GSK-3β (Ser9)/total GSK-3 (D, I, N & S) and pERK (42/44)/total ERK (E, J, O & T). Significant differences between the groups were calculated using two-tailed, unpaired students t-test; *p<0.05, **p<0.01 and ***p<0.001.

3.5. Impaired insulin signaling at the blood-brain barrier in APP/PS1 and HFD fed mice:

As the blood-brain barrier regulates entry and exit of Aβ peptides, various studies reported the crucial role of the BBB in Aβ clearance from the brain. We aimed to understand the effects of APP/PS1 transgene and HFD contribution to insulin mediated responses at the BBB. Upon saline or insulin stimulation brains were quickly perfused to remove the blood cells and were harvested for microvasculature (Reference). The isolated microvasculature was subjected to immunoblotting and probed with various antibodies to analyze insulin signaling events. IRS-1 levels were diminished (p=0.06) upon insulin administration in APP/PS1 male mice of both the feeding regimens (Figure 10F). However, no changes in IRS-1 levels were observed in HFD fed NTg mice upon insulin administration in both the sexes (Figures 10A –P). Interestingly, insulin administration increased IR-β levels in male APP/PS1 and NTg mice fed with HFD (Figure 10G). However, no changes at the level of IR-β were observed in female mice of both the genotypes (Figure 10L & Q). High levels of pAKT were observed in APP/PS1 and HFD fed NTg mice under saline treatment (Figures 10 C & I), upon insulin treatment pAKT levels were further upregulated in HFD fed male mice of both the genotypes (Figure 10H). Upregulation in pAKT levels were observed in female APP/PS1 and HFD mice upon insulin injection (Figure 10R). Furthermore, pGSK-3 levels correlated with the pAKT levels in both APP/PS1 and NTg mice of both the sexes upon insulin administration (Figure 10I & S). Significantly high levels of pERK levels were observed in APP/PS1 male and female mice of both the feeding regimens (Figures 10E & O), insulin administration reduced the ERK levels to control levels in both the sexes (Figures 10J & T).

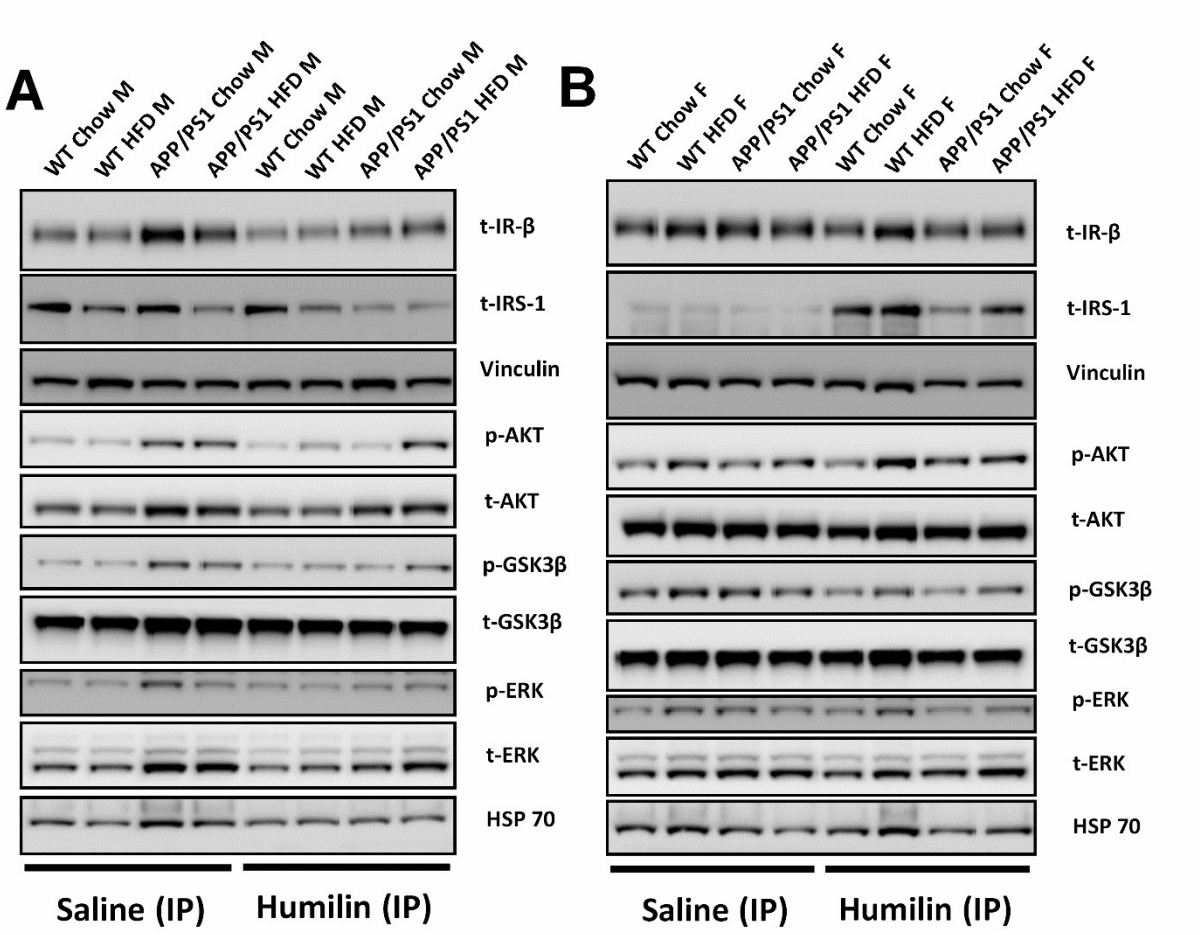

Figure 9: At the end of 16 week feeding, Male and female; APP/PS1 and NTg mice were administered with either 2 IU/Kg insulin or saline (IP) for 20 minutes, animals were sacrificed, vital organs were harvested, proteins were isolated and subjected to western blotting, analyzed for proteins involved in insulin signaling. Representative western blots of microvascular insulin signaling was demonstrated in figure 9.

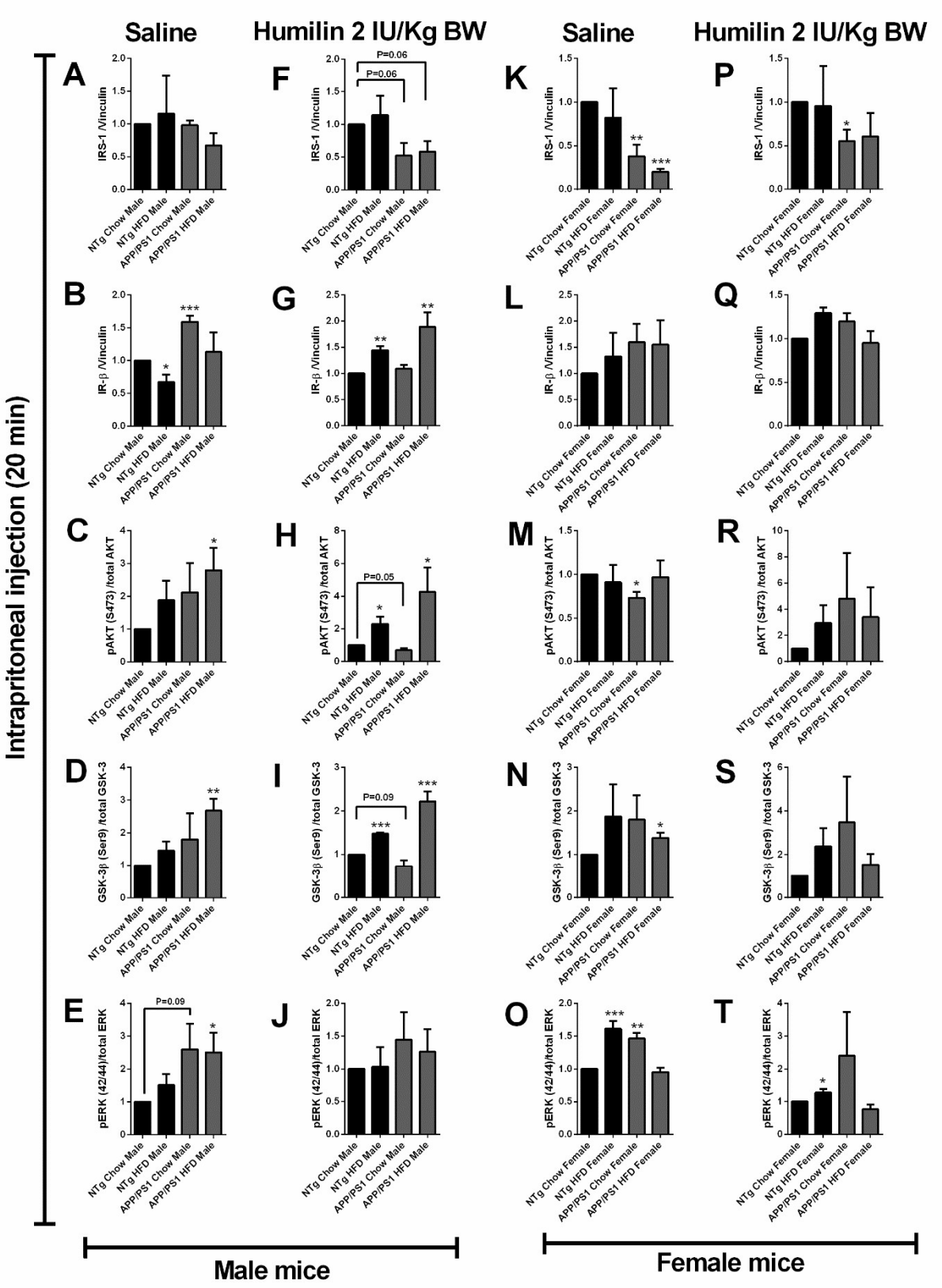

Figure 10: At the end of 16 week feeding, Male and female; APP/PS1 and NTg mice were administered with either 2 IU/Kg insulin or saline (IP) for 20 minutes, animals were sacrificed, vital organs were harvested, proteins were isolated and subjected to western blotting, analyzed for proteins involved in insulin signaling. Quantitative analysis of figure 9 was

performed using ImageJ©. IRS-1/Vinculin (A, F, K & P), IR-β/Vinculin (B, G, L & Q), pAKT (S473)/total AKT (C, H, M & R), GSK-3β (Ser9)/total GSK-3 (D, I, N & S) and pERK (42/44)/total ERK (E, J, O & T). Significant differences between the groups were calculated using two-tailed, unpaired students t-test; *p<0.05, **p<0.01 and ***p<0.001.

3.6. Impaired insulin uptake in APP/PS1 animals:

The clearance and AUC of ^{125}I-insulin in APP/PS1 mice was significantly increased and decreased respectively, as compared to WT mice. when the data from the plasma concentration profiles were input into a two-compartmental model on SAAM II© and analyzed with initial estimates for V, k12 and k21 (two-compartmental distribution rate constants.

3.6.1. Table 1:

Plasma pharmacokinetic parameters	WT	APP/PS1	Statistics
Clearance, CL (Mean ± SD) (ml/min)	0.30 ± 0.05	0.73 ± 0.35	p<0.01
Area under the curve, AUC (µCi.min/ml)	332.9 ± 59.1	136.0 ± 64.3	p<0.05

3.6.2. Clearance and AUC of intravenously injected ^{125}I-insulin in APP/PS1 and WT mice.

Parameter estimates for clearance and AUC were obtained from two-compartmental analyses of data averaged from the plasma concentration profile of 6-month old WT (n=6) and APP/PS1 (n=6).

Following the observations of lowered peripheral insulin levels (increased clearance) in male APP/PS1 mice, brain uptake of 500 µCi of intravenously administered ^{125}I-insulin in APP/PS1 mice was measured by the SPECT/CT imaging protocol. Within the first three minutes after administration of ^{125}I-insulin, it is assumed the radioactivity in the brain parenchyma is insignificant. The brain radioactivity can thus be attributed to ^{125}I-insulin binding to its receptor at the cerebrovascular endothelium. The kinetic curves presented in Fig. 11 have

clearly demonstrated that ^{125}I-insulin binding in WT mice was significantly higher than that observed in APP/PS1 mice. Except the earliest data point, the ^{125}I-insulin radioactivity was substantially greater in WT mice (n=5) than in APP/PS1 (n=4) mice (*p<0.05, two-tailed t-test).

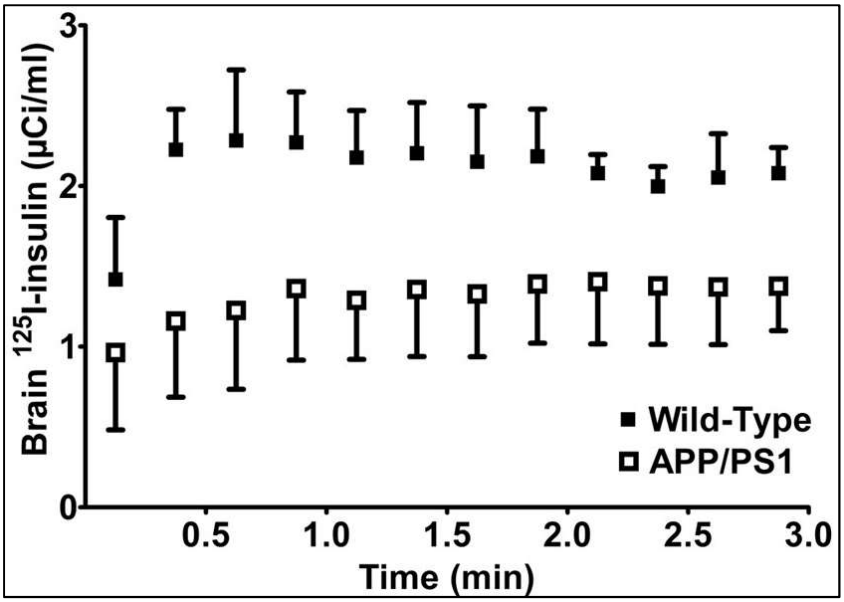

Figure 11: Brain uptake of ^{125}I-insulin (µCi/ml) is plotted against time for NTg and APP/PS1 mice. 500 µCi of ^{125}I-insulin was injected via the femoral vein into and the brain uptake was measured every 12 seconds by SPECT. The brain concentrations of ^{125}I-insulin were corrected for the vascular component by subtracting the brain concentrations by the vascular concentrations (obtained by multiplying the plasma concentration at each time point by the vascular volume). The vascular volume was calculated by normalizing the amount of ^{125}I-insulin in the vasculature by the plasma concentration at the last measured time point. The vascular amount was obtained by subtracting the perfused brain amount from the brain amount at the last measured time point.

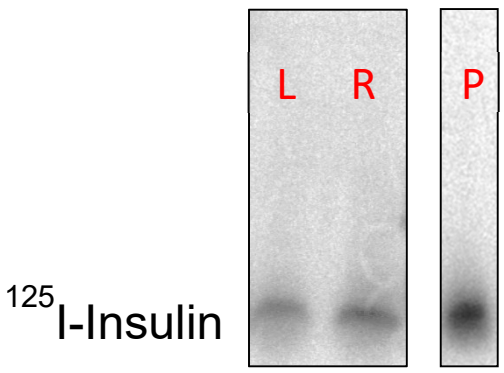

Figure 12. 250 uCi of ^{125}I-Insulin was administered via IV bolus injection. At the end of 60 min, plasma sample was obtained and the mouse was perfused. Then left and right hemispheres

of brain was isolated. The protein content in the plasma and brain samples was resolved by 12% bis-tris SDS page gels. Then, autoradiography (phosphor-imager plate) was performed to visualize the integrity of ^{125}I-Insulin. These results indicate ^{125}I-Insulin is stable in brain and plasma at the measured times.

3.7. Reduced cerebral uptake and accelerated clearance of ^{125}I-Aβ42 in APP/PS1 mice:

Uptake of ^{125}I-Aβ42 was imaged by dynamic SPECT/CT. The rate of uptake of ^{125}I-Aβ42 into brain and peripheral organs such as heart were assessed. The plots of ^{125}I-Aβ42 radioactivity against time depicted in Fig. 13 demonstrated that the brain uptake of ^{125}I-Aβ42 in APP/PS1 (AD) mice was not significantly different from that in WT mice. However, the overall brain accumulation at the end of 40 min showed in Fig.14 suggests that ^{125}I-Aβ42 accumulates more in AD brain than in WT brain. These seemingly contradicting observations indicate that ^{125}I-Aβ42 interacts with the BBB endothelium to an equal extent in both AD and WT mice. However, the transcytosis of ^{125}I-Aβ42, which was shown to be regulated by insulin in our previous studies, is substantially lower in AD mice than in WT mice. Similar trends were also observed in peripheral tissues such as heart (Fig. 15), which is used as a surrogate measure of plasma radioactivity in SPECT/CT imaging.

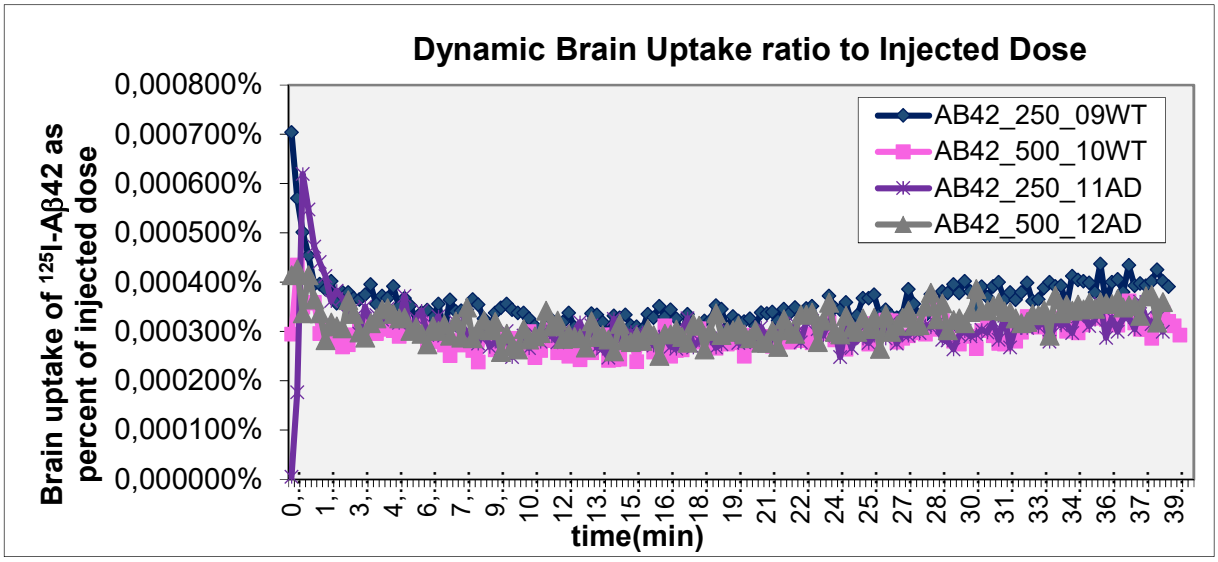

Figure 13: Brain distribution of ^{125}I-Aβ42 (AB42) normalized by the injected dose in wild type (WT) and APP/PS1 (AD) mice. Two doses of 250 and 500 μCi of ^{125}I-Aβ42 were injected to mice via femoral vein and the dynamic SPECT/CT imaging was conducted upto 40 min.

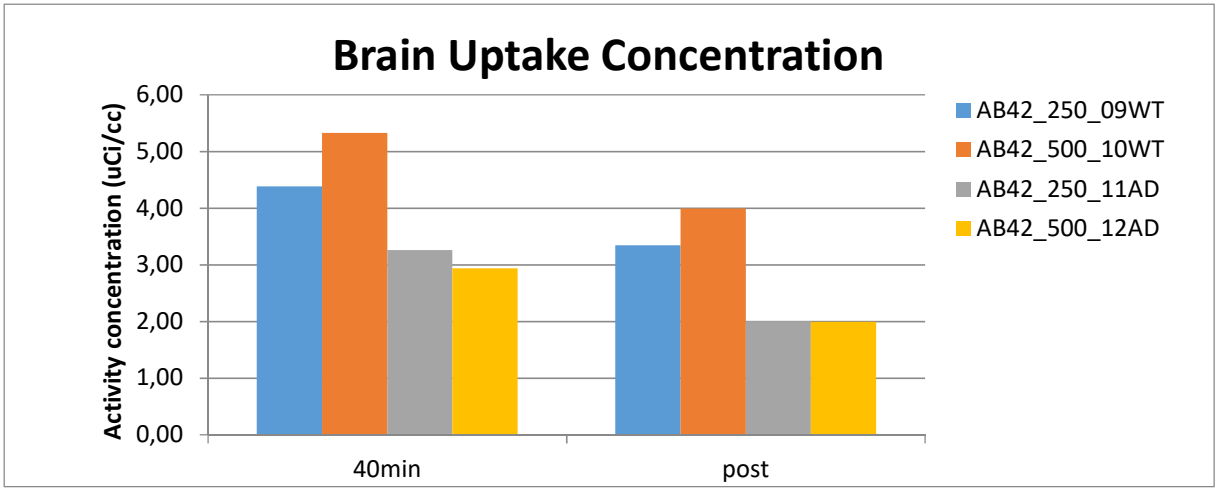

Figure 14: Brain accumulation of ^{125}I-Aβ42 at the end of experiment depicted in Fig.13. The animal was transcardially perfused at the end of 40 min. The brain was harvested from the cranial cavity and the ^{125}I radioactivity was determined in a dual channel gamma counter.

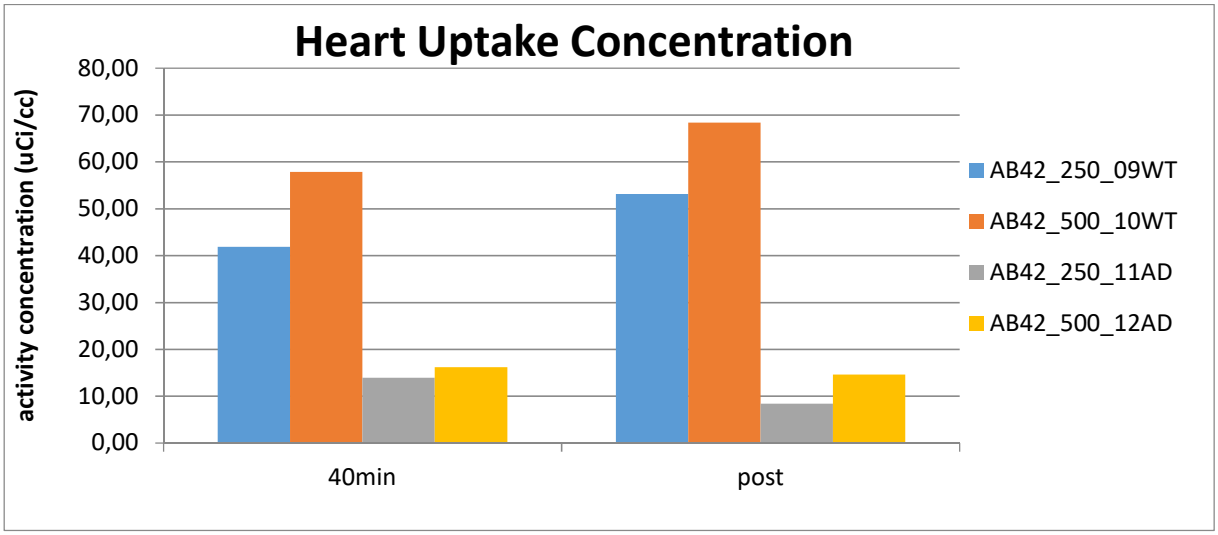

Figure 15: Heart accumulation of ^{125}I-Aβ42 at the end of experiment depicted in Fig.13. The animal was transcardially perfused at the end of 40 min, heart was removed from the thoracic cavity, and the ^{125}I radioactivity was determined in a dual channel gamma counter.

4. DISCUSSION

T2D and obesity are the two major risk factors for AD, the etiology common to both these diseases is manifested as impaired lipid homeostasis, hyperinsulinemia, and insulin resistance (23,24). Apart from mediating metabolic functions in the system, insulin is known to regulate: 1) central Aβ metabolism by modulating the genes and enzymes involved in APP processing and preserving long term memory, prominently in hippocampal neurons (55). 2) clearance of Aβ in the periphery by regulating LRP-1 kinetics, major uptake receptor for Aβ in the liver kinetics in the hepatocytes (56). Central insulin resistance is observed in AD subjects (57), which is also emulated by AD mouse models that exhibited insulin dysregulation at receptor level as well in the downstream insulin signaling.

Recent findings demonstrate that BBB plays a pivotal role in clearing Aβ from brain, and BBB augments Aβ accumulation (39). Impaired function of Aβ receptors at the BBB could lead enhancement in brain Aβ accumulation. Previous studies have demonstrated that Aβ trafficking at the BBB is influenced by peripherally administered insulin, which influences Aβ metabolism and trafficking at multiple levels (40). We aimed to understand the physiological effect of insulin on Aβ clearance at the BBB and how it is impacted under AD and T2D conditions. Up on HFD feeding insulin resistance was induced in APP/PS1 and NTg mice. This was tested by employing insulin tolerance test, which indicated worsened insulin resistance (Figure 1A - F). Interestingly, chow fed APP/PS1 male mice also demonstrated impaired insulin tolerance (Figure 2A & C) and HFD further worsened insulin tolerance in both the male and female APP/PS1 mice compared to NTg mice (Figure 2B & 3B). These results demonstrated the role of HFD in the induction of peripheral insulin resistance. Western blots of the liver lysates from APP/PS1 and NTg coincided with the insulin tolerance data, represented by reduced IRS-1 levels and dysregulated downstream insulin signaling indicated by low pAKT and pGSK-3 up on insulin stimulation. These results indicate the induction of hepatic insulin resistance in HFD fed APP/PS1 and NTg mice (Figure 5 & 6). Moreover, reduced hepatic insulin sensitivity in HFD fed mice is also associated with impaired surface mobilization of LRP-1 in response to insulin exposure. Since, LRP1 plays a crucial role in trafficking Aβ proteins, these changes in LRP1 response may impact peripheral clearance of Aβ.

Liver LRP-1 and deregulated IR-β levels clearly imply that in APP/PS1 mice, a s

Furthermore, changes in peripheral insulin resistance coincided with central insulin signaling deficiencies represented by diminished upstream (pIRS-1 and pIR-β levels) and downstream (pAKT and pGSK3-β levels) regulators of insulin signaling in APP/PS1 mice compared to chow diet fed NTg mice (Figure 7 & 8), indicating that brain insulin resistance in AD is independent of HFD feeding. HFD feeding further worsened central insulin sensitivity, represented by low upstream (pIRS-1 and pIR-β) and downstream (pAKT and pGSK3-β) regulators of insulin signaling, right after stimulation with insulin (Figure 7 & 8). Loss of insulin sensitivity in APP/PS1 mice are in line with recent studies reporting insulin signaling deficiencies in various AD mouse models (58).

Having understood that APP/PS1 mice exhibit central and peripheral insulin signaling deficiencies and HFD feeding further aggravate signaling deficiencies, we next explored the impact of diabetic environment on insulin signaling changes in isolated micro vessels, which represent the BBB, which regulates central Aβ clearance. We identified similar disturbances in microvascular insulin signaling as in central and peripheral compartments, represented by loss in IR-β and IRS-1 levels up on insulin stimulation in APP/PS1 and HFD fed mice (Figure 9 & 10). Moreover, diminished downstream insulin signaling was identified in APP/PS1 and HFD fed mice (Figure 9 & 10). Since, insulin can stimulate the surface mobilization of the LRP-1 at the BBB and contribute to trafficking of Aβ between brain and periphery (40). Our results confirm that under AD and HFD conditions the insulin mediated effects might get compromised because of insulin resistance, thereby contributing to enhanced accumulation of Aβ in the brain.

Insulin is take up from the periphery via insulin receptor mediated endocytosis at the BBB, primarily resided in the lipid rafts (56). Since APP/PS1 mice demonstrated loss of insulin sensitivity and mediated signaling in the brain and at the BBB, studies using dynamic SPECT imaging revealed that insulin uptake is significantly dysregulated in AD mice (Figure 11). More importantly, we observed a significant increase in the rate of clearance of injected ^{125}I-insulin in APP/PS1 mice (Table 1). These observations coincide with the loss of brain and BBB insulin signaling. These findings further strengthen the fact that AD is a form of diabetes of brain and the role of insulin receptors in brain insulin uptake. Diminished insulin uptake in the brain can lead to impaired metabolic and cognitive functions in AD.

Aβ is actively transported across the blood-brain barrier via surface receptors at the BBB, more importantly by receptor for advanced glycation end products (RAGE). Several transporters are identified as potential ligands for Aβ interaction. Since AD subjects display altered BBB homeostasis, we aimed to understand the uptake of soluble ^{125}I-Aβ42 injected via the femoral vein. Using SPECT dynamic imaging we uncovered that similar to insulin soluble Aβ42 uptake is significantly altered in APP/PS1 mice (Figure 14 & 15). More importantly, APP/PS1 mice displayed lower Aβ42 counts in heart, suggesting faster clearance or higher accumulation of peripherally administered soluble ^{125}I-Aβ42 in AD mice, thereby contributing to low Aβ42 uptake in brain (Figure 14). Since Aβ as monomers can be actively taken up and metabolized degrading enzymes like IDE and neprilysin, which are abundant in peripheral organs and liver. APP/PS1 mice display diabetic phenotype with altered insulin levels, we speculate the increased insulin degrading enzyme levels under diabetic conditions could cleave the peripherally administered Aβ, thereby contributing to enhanced metabolism in APP/PS1 mice. The implications of pathological Aβ (oligomers and plaques) may have a different uptake pattern, which needs to be analyzed to further understand the complex environment in APP/PS1 mice.

In conclusion, we identified severely impaired peripheral and central insulin metabolism and function in APP/PS1 mice. Impaired central and BBB insulin resistance contributed to lower insulin and Aβ uptake in APP/PS1 mice. HFD feeding further aggravated the peripheral insulin resistance in APP/PS1 mice. Our studies using SPECT imaging clarified some aspects of implications of AD on brain and BBB insulin uptake. Furthermore, some unusual findings were made regarding Aβ42 uptake under healthy and AD conditions, these findings need to be thoroughly validated and understood in different AD models.

5. REFERENCES

1. Fraser PE, Lévesque L, McLachlan DR. Biochemistry of Alzheimer's disease amyloid plaques. Clin Biochem. 1993 Oct;26(5):339-49.
2. Gouras GK, Olsson TT, Hansson O. β-Amyloid peptides and amyloid plaques in Alzheimer's disease. Neurotherapeutics. 2015 Jan;12(1):3-11.
3. Brion JP. Neurofibrillary tangles and Alzheimer's disease. Eur Neurol. 1998 Oct;40(3):130-40.
4. Takashima A. Amyloid-beta, tau, and dementia. J Alzheimers Dis. 2009;17(4):729-36.
5. Serrano-Pozo A, Frosch MP, Masliah E, Hyman BT. Neuropathological Alterations in Alzheimer Disease. Cold Spring Harbor Perspectives in Medicine: 2011;1(1):a006189.
6. Jahn H. Memory loss in Alzheimer's disease. Dialogues in Clinical Neuroscience. 2013;15(4):445-454.
7. Chow VW, Mattson MP, Wong PC, Gleichmann M. An Overview of APP Processing Enzymes and Products. Neuromolecular medicine. 2010;12(1):1-12. doi:10.1007/s12017-009-8104-z.
8. Sennvik K, Bogdanovic N, Volkmann I, Fastbom J, Benedikz E. Beta-secretase-cleaved amyloid precursor protein in Alzheimer brain: a morphologic study. J Cell Mol Med. 2004 Jan-Mar;8(1):127-34.
9. Kume H, Sekijima Y, Maruyama K, Kametani F. gamma-Secretase can cleave amyloid precursor protein fragments independent of alpha- and beta-secretase pre-cutting. Int J Mol Med. 2003 Jul;12(1):57-60.
10. Zhang Y, Thompson R, Zhang H, Xu H. APP processing in Alzheimer's disease. Molecular Brain. 2011;4:3. doi:10.1186/1756-6606-4-3.
11. Guo Q, Li H, Gaddam SS, Justice NJ, Robertson CS, Zheng H. Amyloid precursor protein revisited: neuron-specific expression and highly stable nature of soluble derivatives. J Biol Chem. 2012 Jan 20;287(4):2437-45.
12. Nicolas G, Wallon D, Goupil C, et al. Mutation in the 3'untranslated region of APP as a genetic determinant of cerebral amyloid angiopathy. European Journal of Human Genetics. 2016;24(1):92-98. doi:10.1038/ejhg.2015.61.
13. Lanoiselée H-M, Nicolas G, Wallon D, et al. APP, PSEN1, and PSEN2 mutations in early-onset Alzheimer disease: A genetic screening study of familial and sporadic cases. Miller BL, ed. PLoS Medicine. 2017;14(3):e1002270.
14. Sellal F, Wallon D, Martinez-Almoyna L, Marelli C, Dhar A, Oesterlé H, Rovelet-Lecrux A, Rousseau S, Kourkoulis CE, Rosand J, DiPucchio ZY, Frosch M, Gombert C, Audoin B, Miné M,

Riant F, Frebourg T, Hannequin D, Campion D, Greenberg SM, Tournier-Lasserve E, Nicolas G. APP Mutations in Cerebral Amyloid Angiopathy with or without Cortical Calcifications: Report of Three Families and a Literature Review. J Alzheimers Dis. 2017;56(1):37-46.

15. Gu L, Guo Z. Alzheimer's Aβ42 and Aβ40 peptides form interlaced amyloid fibrils. Journal of neurochemistry. 2013;126(3):305-311.
16. Iqbal K, Liu F, Gong C-X, Grundke-Iqbal I. Tau in Alzheimer Disease and Related Tauopathies. Current Alzheimer research. 2010;7(8):656-664.
17. Wang JZ, Xia YY, Grundke-Iqbal I, Iqbal K. Abnormal hyperphosphorylation of tau: sites, regulation, and molecular mechanism of neurofibrillary degeneration. J Alzheimers Dis. 2013;33 Suppl 1:S123-39.
18. Wen Y, Planel E, Herman M, Figueroa HY, Wang L, Liu L, Lau LF, Yu WH, Duff KE. Interplay between cyclin-dependent kinase 5 and glycogen synthase kinase 3 beta mediated by neuregulin signaling leads to differential effects on tau phosphorylation and amyloid precursor protein processing. J Neurosci. 2008 Mar 5;28(10):2624-32.
19. Terwel D, Muyllaert D, Dewachter I, Borghgraef P, Croes S, Devijver H, Van Leuven F. Amyloid activates GSK-3beta to aggravate neuronal tauopathy in bigenic mice. Am J Pathol. 2008 Mar;172(3):786-98.
20. Chen G, Ward BD, Xie C, et al. Classification of Alzheimer Disease, Mild Cognitive Impairment, and Normal Cognitive Status with Large-Scale Network Analysis Based on Resting-State Functional MR Imaging. Radiology. 2011;259(1):213-221. doi:10.1148/radiol.10100734.
21. Mielke MM, Leoutsakos J-M, Corcoran CD, et al. Effects of FDA approved medications for Alzheimer's disease on clinical progression. Alzheimer's & dementia : the journal of the Alzheimer's Association. 2012;8(3):180-187.
22. Cummings J, Lee G, Mortsdorf T, Ritter A, Zhong K. Alzheimer's disease drug development pipeline: 2017. Alzheimer's & Dementia : Translational Research & Clinical Interventions. 2017;3(3):367-384.
23. De la Monte SM, Wands JR. Alzheimer's Disease Is Type 3 Diabetes–Evidence Reviewed. Journal of diabetes science and technology (Online). 2008;2(6):1101-1113.
24. Grillo CA, Piroli GG, Lawrence RC, Wrighten SA, Green AJ, Wilson SP, Sakai RR, Kelly SJ, Wilson MA, Mott DD, Reagan LP. Hippocampal Insulin Resistance Impairs Spatial Learning and Synaptic Plasticity. Diabetes. 2015 Nov;64(11):3927-36.

25. Benedict C, Hallschmid M, Hatke A, Schultes B, Fehm HL, Born J, Kern W. Intranasal insulin improves memory in humans. Psychoneuroendocrinology. 2004 Nov;29(10):1326-34.
26. Adzovic L, Lynn AE, D'Angelo HM, Crockett AM, Kaercher RM, Royer SE, Hopp SC, Wenk GL. Insulin improves memory and reduces chronic neuroinflammation in the hippocampus of young but not aged brains. J Neuroinflammation. 2015 Apr 2;12:63.
27. Liu Y, Liu F, Grundke-Iqbal I, Iqbal K, Gong C-X. Deficient brain insulin signalling pathway in Alzheimer's disease and diabetes. The Journal of pathology. 2011;225(1):54-62.
28. Chua LM, Lim ML, Chong PR, Hu ZP, Cheung NS, Wong BS. Impaired neuronal insulin signaling precedes Aβ42 accumulation in female AβPPsw/PS1ΔE9 mice. J Alzheimers Dis. 2012;29(4):783-91.
29. Kim B, Feldman EL. Insulin resistance as a key link for the increased risk of cognitive impairment in the metabolic syndrome. Experimental & Molecular Medicine. 2015;47(3):e149.
30. Wang X, Yu S, Gao SJ, Hu JP, Wang Y, Liu HX. Insulin inhibits Abeta production through modulation of APP processing in a cellular model of Alzheimer's disease. Neuro Endocrinol Lett. 2014;35(3):224-9.
31. Solano DC, Sironi M, Bonfini C, Solerte SB, Govoni S, Racchi M. Insulin regulates soluble amyloid precursor protein release via phosphatidyl inositol 3 kinase-dependent pathway. FASEB J. 2000 May;14(7):1015-22.
32. Vandal M, White PJ, Tremblay C, St-Amour I, Chevrier G, Emond V, Lefrançois D, Virgili J, Planel E, Giguere Y, Marette A, Calon F. Insulin reverses the high-fat diet-induced increase in brain Aβ and improves memory in an animal model of Alzheimer disease. Diabetes. 2014 Dec;63(12):4291-301.
33. Arnold SE, Arvanitakis Z, Macauley-Rambach SL, Koenig AM, Wang HY, Ahima RS, Craft S, Gandy S, Buettner C, Stoeckel LE, Holtzman DM, Nathan DM. Brain insulin resistance in type 2 diabetes and Alzheimer disease: concepts and conundrums. Nat Rev Neurol. 2018 Mar;14(3):168-181.
34. Greenwood CE, Winocur G. Learning and memory impairment in rats fed a high saturated fat diet. Behav Neural Biol. 1990 Jan;53(1):74-87.
35. Martin SA, Jameson CH, Allan SM, Lawrence CB. Maternal high-fat diet worsens memory deficits in the triple-transgenic (3xTgAD) mouse model of Alzheimer's disease. PLoS One. 2014 Jun 11;9(6):e99226.

36. Knight EM, Martins IVA, Gümüsgöz S, Allan SM, Lawrence CB. High-fat diet-induced memory impairment in triple-transgenic Alzheimer's disease (3xTgAD) mice is independent of changes in amyloid and tau pathology. Neurobiology of Aging. 2014;35(8):1821-1832.
37. Reger MA, Watson GS, Green PS, Wilkinson CW, Baker LD, Cholerton B, Fishel MA, Plymate SR, Breitner JC, DeGroodt W, Mehta P, Craft S. Intranasal insulin improves cognition and modulates beta-amyloid in early AD. Neurology. 2008 Feb 5;70(6):440-8. Epub 2007 Oct 17. Erratum in: Neurology. 2008 Sep 9;71(11):866.
38. Steen E, Terry BM, Rivera EJ, Cannon JL, Neely TR, Tavares R, Xu XJ, Wands JR, de la Monte SM. Impaired insulin and insulin-like growth factor expression and signaling mechanisms in Alzheimer's disease--is this type 3 diabetes? J Alzheimers Dis. 2005 Feb;7(1):63-80.
39. Reger MA, Watson GS, Green PS, Baker LD, Cholerton B, Fishel MA, Plymate SR, Cherrier MM, Schellenberg GD, Frey WH 2nd, Craft S. Intranasal insulin administration dose-dependently modulates verbal memory and plasma amyloid-beta in memory-impaired older adults. J Alzheimers Dis. 2008 Apr;13(3):323-31.
40. Yang HT, Sheen YJ, Kao CD, Chang CA, Hu YC, Lin JL. Association between the characteristics of metabolic syndrome and Alzheimer's disease. Metab Brain Dis. 2013 Dec;28(4):597-604.
41. Stöhr O, Schilbach K, Moll L, et al. Insulin receptor signaling mediates APP processing and β-amyloid accumulation without altering survival in a transgenic mouse model of Alzheimer's disease. Age. 2013;35(1):83-101. doi:10.1007/s11357-011-9333-2.
42. Freude S, Hettich MM, Schumann C, Stöhr O, Koch L, Köhler C, Udelhoven M, Leeser U, Müller M, Kubota N, Kadowaki T, Krone W, Schröder H, Brüning JC, Schubert M. Neuronal IGF-1 resistance reduces Abeta accumulation and protects against premature death in a model of Alzheimer's disease. FASEB J. 2009 Oct;23(10):3315-24.
43. Gontier G, George C, Chaker Z, Holzenberger M, Aïd S. Blocking IGF Signaling in Adult Neurons Alleviates Alzheimer's Disease Pathology through Amyloid-β Clearance. J Neurosci. 2015 Aug 19;35(33):11500-13.
44. Deane R, Wu Z, Zlokovic BV. RAGE (yin) versus LRP (yang) balance regulates alzheimer amyloid beta-peptide clearance through transport across the blood-brain barrier. Stroke. 2004 Nov;35(11 Suppl 1):2628-31.
45. Deane R, Bell R, Sagare A, Zlokovic B. Clearance of amyloid-β peptide across the blood-brain barrier: Implication for therapies in Alzheimer's disease. CNS & neurological disorders drug targets. 2009;8(1):16-30.

46. Bell RD, Sagare AP, Friedman AE, Bedi GS, Holtzman DM, Deane R, Zlokovic BV. Transport pathways for clearance of human Alzheimer's amyloid beta-peptide and apolipoproteins E and J in the mouse central nervous system. J Cereb Blood Flow Metab. 2007 May;27(5):909-18.
47. Farris W, Mansourian S, Chang Y, Lindsley L, Eckman EA, Frosch MP, Eckman CB, Tanzi RE, Selkoe DJ, Guenette S. Insulin-degrading enzyme regulates the levels of insulin, amyloid beta-protein, and the beta-amyloid precursor protein intracellular domain in vivo. Proc Natl Acad Sci U S A. 2003 Apr 1;100(7):4162-7.
48. Swaminathan SK, Ahlschwede KM, Sarma V, Curran GL, Omtri RS, Decklever T, Lowe VJ, Poduslo JF, Kandimalla KK. Insulin differentially affects the distribution kinetics of amyloid beta 40 and 42 in plasma and brain. J Cereb Blood Flow Metab. 2017 Jan 1:271678X17709709.
49. Tamaki C, Ohtsuki S, Terasaki T. Insulin facilitates the hepatic clearance of plasma amyloid beta-peptide (1 40) by intracellular translocation of low-density lipoprotein receptor-related protein 1 (LRP-1) to the plasma membrane in hepatocytes. Mol Pharmacol. 2007 Oct;72(4):850-5.
50. Kaur A, Patankar JV, de Haan W, Ruddle P, Wijesekara N, Groen AK, Verchere CB, Singaraja RR, Hayden MR. Loss of Cyp8b1 improves glucose homeostasis by increasing GLP-1. Diabetes. 2015 Apr;64(4):1168-79.
51. Boulay AC, Saubaméa B, Declèves X, Cohen-Salmon M. Purification of Mouse Brain Vessels. J Vis Exp. 2015 Nov 10;(105):e53208.
52. Kandimalla KK, Curran GL, Holasek SS, Gilles EJ, Wengenack TM, Poduslo JF. Pharmacokinetic analysis of the blood-brain barrier transport of 125I-amyloid beta protein 40 in wild-type and Alzheimer's disease transgenic mice (APP/PS1) and its implications for amyloid plaque formation. J Pharmacol Exp Ther. 2005 Jun;313(3):1370-8.
53. Lacor PN, Buniel MC, Chang L, Fernandez SJ, Gong Y, Viola KL, Lambert MP, Velasco PT, Bigio EH, Finch CE, et al. Synaptic targeting by Alzheimer’s-related amyloid beta oligomers. J Neurosci. 2004; 24:10191–10200.
54. Poduslo JF, Curran GL, Wengenack TM, Malester B, Duff K. Permeability of proteins at the blood-brain barrier in the normal adult mouse and double transgenic mouse model of Alzheimer's disease. Neurobiol Dis. 2001 Aug;8(4):555-67.
55. Wang X, Yu S, Gao SJ, Hu JP, Wang Y, Liu HX. Insulin inhibits Abeta production through modulation of APP processing in a cellular model of Alzheimer's disease. Neuro Endocrinol Lett. 2014;35(3):224-9.

56. Tamaki C, Ohtsuki S, Terasaki T: Insulin facilitates the hepatic clearance of plasma amyloid beta-peptide (1 40) by intracellular translocation of low-density lipoprotein receptor-related protein 1 (LRP-1) to the plasma membrane in hepatocytes. Mol Pharmacol 2007;72:850-855.
57. Liu Y, Liu F, Grundke-Iqbal I, Iqbal K, Gong CX: Deficient brain insulin signalling pathway in Alzheimer's disease and diabetes. J Pathol 2011;225:54-62.
58. Velazquez R, Tran A, Ishimwe E, Denner L, Dave N, Oddo S, Dineley KT: Central insulin dysregulation and energy dyshomeostasis in two mouse models of Alzheimer's disease. Neurobiol Aging 2017;58:1-13.
59. Gray SM, Aylor KW, Barrett EJ: Unravelling the regulation of insulin transport across the brain endothelial cell. Diabetologia 2017;60:1512-1521.
60. Arnold SE, Lucki I, Brookshire BR, Carlson GC, Browne CA, Kazi H, Bang S, Choi BR, Chen Y, McMullen MF, Kim SF. High fat diet produces brain insulin resistance, synaptodendritic abnormalities and altered behavior in mice. Neurobiol Dis. 2014 Jul;67:79-87.
61. Plum L, Schubert M, Brüning JC. The role of insulin receptor signaling in the brain. Trends Endocrinol Metab. 2005 Mar;16(2):59-65.
62. Blázquez E, Velázquez E, Hurtado-Carneiro V, Ruiz-Albusac JM. Insulin in the Brain: Its Pathophysiological Implications for States Related with Central Insulin Resistance, Type 2 Diabetes and Alzheimer’s Disease. Frontiers in Endocrinology. 2014;5:161. doi:10.3389/fendo.2014.00161.